

# Measuring model variability using robust non-parametric testing\*

Sinjini Banerjee<sup>1</sup>, Tim Marrinan<sup>2</sup>, Reilly Cannon<sup>2</sup>, Tony Chiang<sup>2</sup>, and Anand D. Sarwate<sup>1</sup>

<sup>1</sup>Department of Electrical and Computer Engineering, Rutgers University

<sup>2</sup>Pacific Northwest National Lab

sb1977@rutgers.edu, {timothy.marrinan,reilly.cannon}@pnnl.gov,

tonychiang.phd@gmail.com, anand.sarwate@rutgers.edu

June 13, 2024

## Abstract

Training a deep neural network often involves stochastic optimization, meaning each run will produce a different model. The seed used to initialize random elements of the optimization procedure heavily influences the quality of a trained model, but this may be obscure from many commonly reported summary statistics, like accuracy. For example, two classification models with identical validation accuracy may disagree on many predicted labels, suggesting that the models have learned two fundamentally different functions. Thus, optimizing over the space of random seeds can lead to higher-quality models, much like optimizing over other hyper-parameters, such as learning rate or regularization parameters, can lead to higher-quality models. However, random seed is often not included in hyper-parameter optimization, perhaps because the relationship between seed and model quality is hard to describe. It is also unknown whether the potential marginal quality improvement of training an additional model with a different random seed is worth the increased computational cost. This work attempts to describe the relationship between deep net models trained with different random seeds and the behavior of the *expected* model. We adopt robust hypothesis testing to propose a novel summary statistic for network similarity, referred to as the  $\alpha$ -trimming level. Our contributions are two-fold. First, we use the  $\alpha$ -trimming level to show that the empirical cumulative distribution function of an ensemble model created from a collection of trained models with different random seeds approximates the average of these functions as the number of models in the collection grows large. This insight provides guidance for how many random seeds should be sampled to ensure that an ensemble of these trained models is a reliable representative. Second, we show that the  $\alpha$ -trimming level is more expressive than different performance metrics like validation accuracy, churn, or expected calibration error when taken alone and may help with random seed selection in a more principled fashion. We demonstrate the value of the proposed statistic in real experiments and illustrate the advantage of fine-tuning over random seed with an experiment in transfer learning.

---

\*This work was partially supported by the Statistical Inference Generates kNowledge for Artificial Learners (SIGNAL) program at Pacific Northwest National Laboratory (PNNL), as well as by the Mathematics for Artificial Reasoning in Science (MARS) initiative via the Laboratory Directed Research and Development (LDRD) Program at PNNL. PNNL is a multi-program national laboratory operated for the U.S. Department of Energy (DOE) by Battelle Memorial Institute under Contract No. DE-AC05-76RL0-1830.

<sup>†</sup>Corresponding author, sb1977@rutgers.edu.

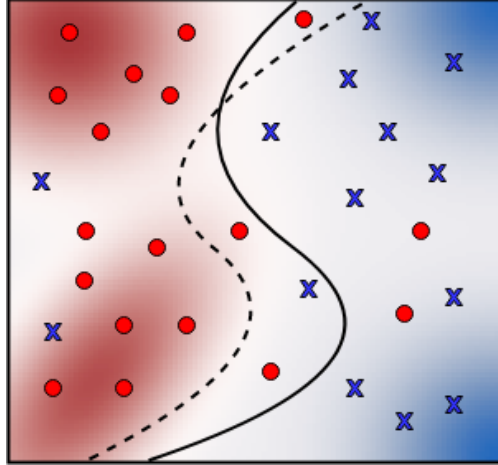


*Figure 1:* Illustration of two models with the same validation accuracy but different decision boundaries.

## 1 Introduction

Deep learning models have achieved state-of-the-art performance on complex tasks in healthcare, education, cyber-security, and other critical domains. Training these models takes significant time, energy, and financial resources. Since training algorithms use stochastic optimization for non-convex objectives, models produced by different training runs, in general, converge to different solutions. These trained models may correspond to different functions, even with a similar objective value and validation/test accuracy. Models are also often continuously retrained as new data arrives. This necessitates algorithmic and architectural changes in state-of-the-art models to improve their performance on new data. The run-to-run variability in training models makes it difficult to conclude if a specific initialization or hyper-parameter tuning made a meaningful difference in model performance or if it just “got lucky” due to the (unavoidable) presence of randomness in the optimization. Without this knowledge, comparing training configurations to assess whether one is better becomes difficult.

Consider the following stylized model of a standard machine learning working process: a practitioner trains  $M$  models with different hyper-parameter settings, chooses the model with the best validation performance (fine-tuning), and evaluates it on test data. This could also involve fine-tuning a model pre-trained on large datasets for a downstream task using a final task-specific layer. In this work, we consider the random seed in the stochastic optimization as a hyper-parameter itself. Gundersen et al. [13] provided a taxonomy of sources of irreproducibility in machine learning practice and identified different seeds controlling model initialization, batch shuffling during mini-batch stochastic gradient descent (SGD), and data sampling as some of the major sources of randomness present in the training procedure. The importance of using random seeds as part of hyper-parameter tuning in deep neural network (DNN) training has been previously highlighted in the literature. Henderson et al. [14], Reimers et al. [30], Melis et al. [24], Bouthillier et al. [7], and Picard et al. [28] all found the effect of random seed on model performance to be statistically significant. Other works have focused on understanding the random seed effect on specific sources of randomness in training. For example, Fort et al. [11] found that initialization has a larger effect than batch order in SGD on model performance, while Bouthillier et al. [6] showed the opposite. Summers and Dinneen [32], and Jordan [18] show that networks converge to vastly different values even with the change of a single bit of network parameters during initialization. While studying

run-to-run variability in pre-trained BERT models over different random seeds, Dodge et al. [8] noted a validation performance gain of 7% over previously reported results, highlighting the importance of fine-tuning over random seed. All the above-mentioned works have assessed the impact randomness has on the *validation accuracy*, or *churn* [25] between models, which quantifies how two models differ in their predictions on the same test point. These summary statistics only focus on the *decisions* made by predictive (classification) models and do not directly assess differences in the functions learned by these models.

In this paper, we assess DNN training variability over random seeds in terms of the *network outputs used to make the decision*. Figure 1 illustrates the difference: the solid and dashed lines represent two decision boundaries between red (circle) and blue (cross). Accuracy measures incorrect decisions, and the churn is determined by the region between the two curves. We are interested in the shaded regions, which show the thresholded network output to make decisions. If we think of the training algorithm as generating a random sample from a function space, we can use other tools to understand model variability. As a first step, we can examine the distribution of the pre-thresholded outputs (the *logit gap*) from functions learned by different runs of a fixed DNN architecture. To that end, we adopt a non-parametric hypothesis testing framework to measure the similarity of functions learned by DNN models that vary in random seeds.

This paper is organized as follows,

- In section 2, we introduce notations and empirical cumulative distribution functions (eCDFs) of interest.
- In section 3, we introduce the classical two-sample Kolmogorov–Smirnov (KS) test to measure the closeness between two models, propose a reference distribution used to formulate the null hypothesis and derive a threshold for this test.
- With the limitations of a classical KS test in mind, in section 4, we formulate a robust version of the two-sample KS test, and propose a measure of closeness/discrepancy referred to as the  $\alpha$ -trimming level between a model and the reference distribution.
- In section 5, we provide empirical evidence that the proposed reference distribution is close to the eCDF of a deep ensemble (a technique used in the machine learning literature to boost model performance and reduce variability). We perform two case studies highlighting the usefulness of our proposed measure of closeness for random seed selection.

## 2 Problem setup

**Notation:** For a positive integer  $n$ , let  $[n] = \{1, 2, \dots, n\}$ . Random variables will be denoted in boldface, with realizations being non-bolded, so  $\boldsymbol{\theta}$  is a random variable and  $\theta$  is a realization. We consider training a DNN for predicting an output taking values in a set  $\mathcal{Z}$  with input from a (feature vector)  $x$  taking values in a space  $\mathcal{X}$ . A DNN with a given architecture is specified by a set of parameters (e.g. the weights)  $\theta$  taking values in parameter space,  $\Theta$ .

We will restrict attention to *binary classification* using a DNN with parameters  $\theta$ . Given a label space  $\mathcal{Y}$ , a training algorithm takes a training set,  $\mathcal{D}_{\text{train}} = \{(x_i, y_i) \in \mathcal{X} \times \mathcal{Y} : i \in [N_{\text{train}}]\}$ , estimates the weights  $\theta$  that (approximately) minimize the empirical loss  $\hat{R}(\theta; \mathcal{D}_{\text{train}})$  over the training data, and assigns a label  $y \in \mathcal{Y}$  using a *softmax* operation. We model this by assuming the DNN takes an input  $x$  and computes functions  $m^+(x | \theta)$  and  $m^-(x | \theta)$ , with the predicted label  $\hat{y}(x; \theta)$  being +1 if  $m^+(x | \theta) \geq m^-(x | \theta)$  and -1 otherwise. A Bayesian interpretation of this rule assumes the data is generated according to an (unknown) distribution  $\pi(x, y)$ , with a likelihood function

$\bar{\pi}(x|y)$ , and a uniform prior  $\text{Unif}[\mathcal{Y}]$ . The functions  $m^+(x|\theta)$  and  $m^-(x|\theta)$  for the positive and negative classes can be converted into posterior probability estimates:

$$\hat{\pi}(y = 1 | x) = \frac{\exp(m^+(x|\theta))}{\exp(m^+(x|\theta)) + \exp(m^-(x|\theta))}. \quad (1)$$

$$\hat{\pi}(y = -1 | x) = \frac{\exp(m^-(x|\theta))}{\exp(m^+(x|\theta)) + \exp(m^-(x|\theta))}. \quad (2)$$

The prediction function is then the maximum *a posteriori* (MAP) estimate:

$$\hat{y}(x; \theta) = \text{sgn}(\hat{\pi}(y = 1 | x) - \hat{\pi}(y = -1 | x)) = \text{sgn}(m^+(x|\theta) - m^-(x|\theta)). \quad (3)$$

We can then assume the learned function is  $m(x; \theta) = m^+(x|\theta) - m^-(x|\theta)$  which is an approximation to the (unknown) log-likelihood ratio  $\log \frac{\bar{\pi}(x|y=1)}{\bar{\pi}(x|y=-1)}$ . We therefore refer to  $m^+(x|\theta)$  and  $m^-(x|\theta)$  as *logits* and  $m(x; \theta)$  as the *logit gap*. In our setting, for a given  $\theta \in \Theta$ , the network computes the function  $m(x; \theta)$  (logit gap function), and the DNN defines a family of functions  $\mathcal{M} = \{m(x; \theta) : \mathcal{X} \rightarrow \mathcal{Z} : \theta \in \Theta\}$ . The goal of *training* a DNN is to find a “good” setting for the parameters  $\theta$  or, equivalently, to find a “good” function  $m \in \mathcal{M}$ .

DNN training algorithms almost always use *stochastic optimization* for training. The optimization algorithms used in DNN training are approximate in two ways. First, they will generally converge to a local minimum because the risk minimization problem is non-convex. Second, they are usually stochastic, meaning the estimated parameters,  $\theta$ , are random variables. Thus, two runs of the same training algorithm, on the same training set  $\mathcal{D}_{\text{train}}$ , can produce different functions. One natural question is to ask how different these functions are. We can try to answer this using a *test set*,  $\mathcal{D}_{\text{test}} = \{(x_j, y_j) : j \in [N_{\text{test}}]\}$ . If we assume  $\mathcal{D}_{\text{test}}$  is drawn i.i.d. from the data distribution  $\pi$ , then given a trained model  $m(x; \theta)$ , the set of values  $\{m(x_j; \theta) : j \in [N_{\text{test}}]\}$  is also an i.i.d. sample from a distribution on  $\mathbb{R}$  induced by  $\pi$ .

Let  $\tau$  be the distribution of  $\theta$  corresponding to the randomness in the training algorithm run on data set  $\mathcal{D}_{\text{train}}$ . Then  $\mathcal{D}_{\text{param}} = \{\theta_1, \theta_2, \dots, \theta_M\}$  is sampled i.i.d.  $\sim \tau$ . Let  $\mathbb{1}(\cdot)$  denote the indicator function, such that  $\mathbb{1}(x \leq t) = 1$  if  $x \leq t$ , and 0 otherwise. Let  $\mathcal{P}$  be the set of probability measures on  $\mathbb{R}$  and a CDF an element of  $\mathcal{P}$ . Given a fixed DNN architecture, the training set  $\mathcal{D}_{\text{train}}$ , and a stochastic training algorithm, the training algorithm takes the training set  $\mathcal{D}_{\text{train}}$  and uses randomization in several different ways to produce a trained model. Thus, given the set  $\mathcal{D}_{\text{param}}$  sampled i.i.d. from  $\tau$ , these parameters correspond to  $M$  i.i.d. samples,  $\{m(x; \theta_k) : k \in [M]\}$ , taking values in  $\mathcal{M}$ . When the models are applied to  $\mathcal{D}_{\text{test}}$ , they produce  $M$  individual CDFs taking values in  $\mathcal{P}$ , which can be written as,

$$G_k(t) = \mathbb{E}_{\pi|\theta_k}[\mathbb{1}(m(\mathbf{x}; \theta_k) \leq t)] \text{ for } k \in [M]. \quad (4)$$

Without access to the underlying data distribution  $\pi$ , we work with the eCDFs instead, which can be written as,

$$\hat{G}_k(t) = \frac{1}{N_{\text{test}}} \sum_{j=1}^{N_{\text{test}}} \mathbb{1}(m(x_j; \theta_k) \leq t) \text{ for } k \in [M]. \quad (5)$$

The distribution on  $\mathcal{P}$  of the CDFs from the test set is induced by  $\tau \times \pi$ , and the expected CDF is,

$$F_{\tau \times \pi}(t) = \mathbb{E}_{\tau \times \pi}[\mathbb{1}(m(\mathbf{x}; \theta) \leq t)]. \quad (6)$$

Without access to  $\tau \times \pi$ , we can consider an (approximate) empirical version of  $F_{\tau \times \pi}$  if we condition Equation (6) on  $\mathcal{D}_{\text{param}}$ , and get the following conditional expected CDF,

$$\begin{aligned} \hat{F}_{\pi|\mathcal{D}_{\text{param}}}(t) &= \mathbb{E}_{\pi|\mathcal{D}_{\text{param}}} \left[ \frac{1}{M} \sum_{k=1}^M (\mathbb{1}(m(\mathbf{x}; \theta_k) \leq t)) \right] \\ &= \frac{1}{M} \sum_{k=1}^M \mathbb{E}_{\pi|\mathcal{D}_{\text{param}}} [(\mathbb{1}(m(\mathbf{x}; \theta_k) \leq t))], \end{aligned} \quad (7)$$

by the linearity of expectation.

To remove the dependence on the underlying data distribution  $\pi$ , we further look at an empirical version of  $\hat{F}_{\pi|\mathcal{D}_{\text{param}}}$ , by taking the average of eCDFs of  $M$  individually trained models,

$$\hat{G}(t) = \frac{1}{M} \sum_{k=1}^M \left( \frac{1}{N_{\text{test}}} \sum_{j=1}^{N_{\text{test}}} \mathbb{1}(m(x_j, \theta_k) \leq t) \right). \quad (8)$$

In contrast with  $\hat{G}$ , which is the average of individual eCDFs, we can also sample  $P$  models from our collection of  $M$  models and construct an ensemble model,  $\bar{m}(x_j) = \frac{1}{P} \sum_{k=1}^P m(x_j, \theta_k)$ , by averaging their logit gaps. The eCDF of this ensemble model can then be written as,

$$\hat{G}_e(t) = \frac{1}{N_{\text{test}}} \sum_{j=1}^{N_{\text{test}}} \mathbb{1} \left( \frac{1}{P} \sum_{k=1}^P m(x_j, \theta_k) \leq t \right), k \in M. \quad (9)$$

Given the test set, our central object of inquiry is the empirical distribution of logit gaps as defined in (5). We can control which sources of randomness are used in the training by switching on or off these different sources. For example, we can use deterministic initialization or fixed batch ordering. Under these scenarios, we can generate  $M$  models and analyze the variability of these models with respect to (w.r.t.) a reference function, representative of what the group has learned in consensus.

### 3 Kolmogorov-Smirnov test to analyze model variability

We use a framework from non-parametric hypothesis testing to measure how different the models are. Ideally, we would want to analyze variability in the training procedure by measuring the closeness of the eCDF of a trained model  $\hat{G}_k$  defined in Equation (5) to their expected CDF  $F_{\tau \times \pi}$  defined in Equation (6). However, without access to  $\tau \times \pi$ , we consider the expected CDF  $\hat{F}_{\pi|\mathcal{D}_{\text{param}}}$  conditioned over  $\mathcal{D}_{\text{param}}$  as defined in Equation (7). If we had access to  $\hat{F}_{\pi|\mathcal{D}_{\text{param}}}$ , we could assess whether or not a given model  $m(x; \theta_k)$  is a representative sample from the training algorithm by testing if the model's eCDF  $\hat{G}_k$  is close to  $\hat{F}_{\pi|\mathcal{D}_{\text{param}}}$ . This can be achieved through the following hypothesis test,

$$\begin{aligned} \mathcal{H}_0: \{m(x_j; \theta_k): j \in [N_{\text{test}}]\} &\sim \hat{F}_{\pi|\mathcal{D}_{\text{param}}} \\ \mathcal{H}_1: \{m(x_j; \theta_k): j \in [N_{\text{test}}]\} &\not\sim \hat{F}_{\pi|\mathcal{D}_{\text{param}}}, \end{aligned} \quad (10)$$

where  $\mathcal{H}_0$ , and  $\mathcal{H}_1$  are the null, and alternate hypothesis. However, in our application, we also do not have access to  $\hat{F}_{\pi|\mathcal{D}_{\text{param}}}$ . Instead, we can use the average of eCDFs from  $M$  models,  $\hat{G}$ , defined in Equation (8), as a proxy to  $\hat{F}_{\pi|\mathcal{D}_{\text{param}}}$ . Thus, our new goal is to test the closeness of  $\hat{G}_k$  to  $\hat{F}_{\pi|\mathcal{D}_{\text{param}}}$  through a hypothesis test using  $\hat{G}$ . In particular, we want to show if  $\hat{G}_k$  is close to  $\hat{G}$  holds

with high probability (w.h.p.), then  $\hat{G}_k$  will also be “close” to  $\hat{F}_{\pi|\mathcal{D}_{\text{param}}}$ , provided w.h.p.  $\hat{F}_{\pi|\mathcal{D}_{\text{param}}}$  is close to  $\hat{G}$ . Thus, without direct access to  $\hat{F}_{\pi|\mathcal{D}_{\text{param}}}$ , the KS-test to detect whether  $m(x; \theta_k)$  has been drawn from  $\hat{F}_{\pi|\mathcal{D}_{\text{param}}}$  requires three steps,

- Step 1: We show that the distance between  $\hat{F}_{\pi|\mathcal{D}_{\text{param}}}$  and  $\hat{G}$  can be bounded w.h.p. using the DKW inequality and a union bound over the collection of parameters.
- Step 2: We choose  $\hat{G}$  as the reference function and apply a two-sample KS-test to determine if samples from  $\hat{G}$  and  $\hat{G}_k$  have been drawn from the same distribution.
- Step 3: Finally, we conclude that if samples from  $\hat{G}$  and  $\hat{G}_k$  have indeed been drawn from the same distribution, i.e., if  $\hat{G}_k$  is close to  $\hat{G}$ , then  $\hat{G}_k$  is also close to  $\hat{F}_{\pi|\mathcal{D}_{\text{param}}}$ , by combining the thresholds in Step 1 and Step 2.

To show that Step 1 holds, in section 7.1 of the Appendix, we develop an analysis that results in the following theorem,

**Theorem 1.** *Let  $\hat{G}$  and  $\hat{F}_{\pi|\mathcal{D}_{\text{param}}}$  be given by Equation (8) and (7). Then for any  $\delta_b > 0$ ,*

$$\mathbb{P}_{\pi|\mathcal{D}_{\text{param}}} \left( \left\| \hat{F}_{\pi|\mathcal{D}_{\text{param}}} - \hat{G} \right\|_{\infty} > \delta_b \right) \leq \epsilon_b, \quad (11)$$

,where  $\epsilon_b = 2M \exp(-2N_{\text{test}}\delta_b^2)$ .

After proving Step 1, we proceed to Step 2, where we would like to test the binary hypothesis whether samples from  $\hat{G}_k$  and  $\hat{G}$  have been drawn from the same distribution through the following two-sample hypothesis test,

$$\begin{aligned} \tilde{\mathcal{H}}_0: & \hat{G}, \hat{G}_k \text{ are the same distribution} \\ \tilde{\mathcal{H}}_1: & \hat{G}, \hat{G}_k \text{ are not the same distribution,} \end{aligned} \quad (12)$$

where  $\tilde{\mathcal{H}}_0$ , and  $\tilde{\mathcal{H}}_1$  are the null, and alternate hypothesis. A two-sample KS test can solve the above problem, with the two-sample DKW inequality setting a threshold for the test [33],

$$\mathbb{P}_{\pi|\mathcal{D}_{\text{param}}} \left( \left\| \hat{G} - \hat{G}_k \right\|_{\infty} > \delta_a \right) \leq \epsilon_a, \quad (13)$$

where  $\epsilon_a = C \exp(-2(\frac{mn}{m+n})\delta_a^2)$ ,  $m, n$  are the number of i.i.d. samples from  $\hat{G}$  and  $\hat{G}_k$  respectively, and  $m = n = \frac{N_{\text{test}}}{2}$ . For  $m = n \geq 458$ , the leading constant  $C$  can be replaced with 2, as shown by Wood et. al. [33, Theorem c]. By fixing  $\epsilon_a$  we can set the threshold as,

$$\delta_a = \sqrt{\frac{2}{N_{\text{test}}} \ln \frac{2}{\epsilon_a}}. \quad (14)$$

For models not rejected under  $\tilde{\mathcal{H}}_0$ , we can use the triangle inequality to find an upper bound on the  $L_{\infty}$ -distance between  $\hat{G}_k$  and  $\hat{F}_{\pi|\mathcal{D}_{\text{param}}}$  resulting in,

$$\left\| \hat{F}_{\pi|\mathcal{D}_{\text{param}}} - \hat{G}_k \right\|_{\infty} \leq \delta_a + \delta_b. \quad (15)$$

Thus, to test our hypothesis in Equation (10), we carry out the following two-sample KS test,

$$\| \hat{G} - \hat{G}_k \|_{\infty} \underset{\tilde{\mathcal{H}}_0}{\overset{\tilde{\mathcal{H}}_1}{\geq}} \delta_a. \quad (16)$$

which implies the following threshold for our original hypothesis,

$$\| \hat{F}_{\pi|\mathcal{D}_{\text{param}}} - \hat{G}_k \|_{\infty} \underset{\mathcal{H}_0}{\overset{\mathcal{H}_1}{\geq}} \delta_a + \delta_b. \quad (17)$$

## 4 Two-sample robust KS test to estimate model variability

In large sample settings, the KS test often rejects the null because even small changes in the sample can result in a significant shift in the  $L_\infty$ -norm [12, p.245]. Note that due to a lack of knowledge about our null distribution or possible ambiguity regarding what the true  $\hat{F}_{\pi|\mathcal{D}_{\text{param}}}$  is, we also do not expect our empirical samples to look exactly like they were drawn from  $\hat{F}_{\pi|\mathcal{D}_{\text{param}}}$ . In this scenario, a classical KS test will likely reject the null even for some samples drawn from  $\hat{F}_{\pi|\mathcal{D}_{\text{param}}}$ . To reduce the number of false rejections, we relax the test to allow for a controlled number of outliers using ideas from *robust statistics* [17].

Consider the following scenario. Let  $\hat{G}_k$  be an independently trained model (candidate model) not rejected under the null hypothesis of our classical KS test in Equation (16) i.e. w.h.p.  $\|\hat{G} - \hat{G}_k\|_\infty \leq \delta_a$ . An upper bound on the  $L_1$ -distance between  $\hat{G}$  and  $\hat{G}_k$  can be established as,

$$\|\hat{G} - \hat{G}_k\|_1 \leq N_{\text{test}}\delta_a. \quad (18)$$

Thus, the null hypothesis of our classical KS test corresponds to an  $L_1$ -ball of radius  $N_{\text{test}}\delta_a$  around  $\hat{G}$  as shown in Figure 2. Consider another candidate model  $\hat{G}_j$ ,  $j \neq k$ , rejected by the KS test in Equation (16). For a small  $\delta$ , the  $L_\infty$ -distance between  $\hat{G}$  and  $\hat{G}_j$  can be bounded by:

$$\delta_a \leq \|\hat{G} - \hat{G}_j\|_\infty \leq \delta_a + \delta. \quad (19)$$

The  $L_1$ -distance between  $\hat{G}$  and  $\hat{G}_j$  can be similarly bounded by:

$$N_{\text{test}}\delta_a \leq \|\hat{G} - \hat{G}_j\|_1 \leq N_{\text{test}}(\delta_a + \delta). \quad (20)$$

Thus, with a robust KS test, we aim to broaden our null hypothesis by including nearby models like  $\hat{G}_j$  that are rejected under the null but within an  $L_1$ -ball slightly greater than  $N_{\text{test}}\delta_a$ . The concept of nearby models was quantified by Huber through contamination neighborhoods [16]. Given a distribution  $P_0 \in \mathcal{P}$  and a scalar,  $\alpha \in [0, 1]$ , the  $\alpha$ -contaminated neighborhood around  $P_0$  is  $\mathcal{V}_\alpha(P_0) = \{(1 - \alpha)P_0 + \alpha Q : Q \in \mathcal{P}\}$ . Alvarez-Esteban et al. [1] introduce a related concept of  $\alpha$ -contaminated neighborhoods as the set of so-called  $\alpha$ -trimmings of  $P \in \mathcal{P}$  defined by,

$$\mathcal{R}_\alpha(P) = \left\{ P^* \in \mathcal{P} : P^* \lll P, \frac{dP}{dP^*} \leq \frac{1}{(1 - \alpha)}P - \text{a.s.} \right\}. \quad (21)$$

Trimmings are related to contamination neighborhoods as [2],

$$P \in \mathcal{V}_\alpha(P_0) \Leftrightarrow P_0 \in \mathcal{R}_\alpha(P). \quad (22)$$

The advantage of using trimming sets to define nearby models, as shown by del Barrio et al. [4] is that we can compute, for a given  $\hat{G}_k$ , the closest  $L_\infty$  approximation to  $\hat{G}$ , in the set of  $\alpha$ -trimmings of  $\hat{G}_k$ :

$$d(\hat{G}, \mathcal{R}_\alpha(\hat{G}_k)) = \min_{\tilde{F} \in \mathcal{R}_\alpha(\hat{G}_k)} \|\hat{G} - \tilde{F}\|_\infty. \quad (23)$$

The core idea behind trimming is to ask if removing a small fraction of samples (from the test set) would allow a KS test to not reject the null hypothesis. We point the readers to Section 7.2, and 7.3 in the Appendix for a detailed description.

Thus, we want to know how much trimming is needed for nearby models like  $\hat{G}_j$ , rejected under a classical KS test, i.e. not included within  $L_1$ -ball of radius  $N_{\text{test}}\delta_a$  around  $\hat{G}$ , to not be rejected

under the null hypothesis. We can think of the trimming level  $\alpha$  as the radius of another  $L_1$ -ball around  $\hat{G}_j$ . Increasing the trimming level is the same as increasing the radius of this ball. We want to know how big the  $L_1$ -ball around  $\hat{G}_j$  needs to be to intersect the  $L_1$ -ball of radius  $N_{\text{test}}\delta_a$  around  $\hat{G}$ . This is demonstrated in a toy diagram in Figure 2. The pink ball is an  $L_1$ -ball (trimming set) of radius  $\alpha'$  around  $\hat{G}_j$ . A trimming level of  $\alpha = \alpha'$  wasn't enough to include the trimmed function  $\tilde{F}$  inside  $N_{\text{test}}\delta_a$  contamination ball of  $\hat{G}$ . But if we increase the radius to create an  $L_1$ -ball of radius  $\alpha = \hat{\alpha}$  around  $\hat{G}_j$ , we see that the optimal trimmed function  $\tilde{F}$  is included within the  $N_{\text{test}}\delta_a$  contamination ball of  $\hat{G}$ . Thus our goal is to increment  $\alpha$  and at each increment run the following hypothesis test,

$$d(\hat{G}, \mathcal{R}_\alpha(\hat{G}_k)) \underset{\mathcal{H}_0}{\overset{\mathcal{H}_1}{\geq}} \delta_a. \quad (24)$$

i.e. if  $\tilde{F}$  is within  $N_{\text{test}}\delta_a$  ball of  $\hat{G}$ .

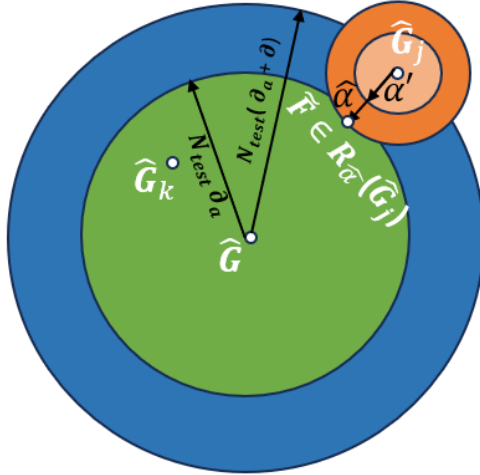


Figure 2: Illustration of  $L_1$ -contamination balls and trimming sets

**Proposed two-sample robust KS test:** To that end, we develop a two-sample version of the robust KS test discussed in Section 4. We use bootstrap sampling to resample  $\frac{N_{\text{test}}}{2}$  i.i.d. test points to compute  $\hat{G}$ , and  $\hat{G}_k$ . Since we only have access to  $\hat{G}$  and not samples from it, let  $\frac{N_{\text{test}}}{2}$  be the number of i.i.d. samples generated from  $\hat{G}$  using inverse transform sampling, and  $z = z_1, z_2, \dots, z_{N_{\text{test}}}$  be the combined ordered arrangement of  $N_{\text{test}}$  samples from  $\hat{G}$ , and  $\hat{G}_k$ . For a fixed  $\alpha$ , we calculate the  $\alpha$ -trimming of  $\hat{G}_k$  that minimizes the  $L_\infty$ -distance to  $\hat{G}$ . Our robust hypothesis test is then,

$$\max_z \min_{\tilde{F} \in \mathcal{R}_\alpha(\hat{G}_k)} |\hat{G}(z) - \tilde{F}(z)| \underset{\mathcal{H}_0}{\overset{\mathcal{H}_1}{\geq}} \delta_a, \quad (25)$$

where  $\delta_a$  can be set as discussed in Equation (13). We use this test in Algorithm 1 to compute the smallest  $\alpha$  for which the test fails to reject  $\mathcal{H}_0$ . The output  $\hat{\alpha}$  is our proposed measure of discrepancy between model  $\hat{G}_k$  and  $\hat{G}$ . We expect candidate models with small  $\hat{\alpha}$  to be similar to those not rejected under the null hypothesis, i.e., the eCDF of these models are expected to all be close to the average of their eCDFs. In Section 5 we demonstrate how  $\hat{\alpha}$  relates to metrics like accuracy and churn, commonly adopted to understand model performance.



---

**Algorithm 1:** Estimate  $\hat{\alpha}$  measure

---

**Data:**  $\mathcal{D}_{\text{test}}$  samples, trained models  $\{m_k: k \in [M]\}$ , candidate model  $m_l \notin [M]$ , threshold  $\delta_a$ , trimming levels  $(\alpha_1, \dots, \alpha_T)$

**Result:** trimming level estimate  $\hat{\alpha}$

**for**  $b = 1$  *to*  $B$  **do**

    Compute  $\hat{G}$  using  $\{m_k: k \in [M]\}$ , and  $\frac{N_{\text{test}}}{2}$  resampled from  $\mathcal{D}_{\text{test}}$ ;

    Compute  $\hat{G}_k$  using  $m_l \notin [M]$ , and  $\frac{N_{\text{test}}}{2}$  resampled from  $\mathcal{D}_{\text{test}}$ ;

    Generate  $\frac{N_{\text{test}}}{2}$  samples from  $\hat{G}$  using inverse transform sampling to form

$z = z_1, z_2, \dots, z_{N_{\text{test}}}$  as the combined ordered arrangement of  $N_{\text{test}}$  samples from  $\hat{G}$ , and  $\hat{G}_k$ .

    Reject  $\leftarrow 1$ ,  $\hat{\alpha} \leftarrow 0$ ,  $t \leftarrow 1$ ;

**while** Reject = 1 *and*  $t \leq T$  **do**

$\alpha \leftarrow \alpha_t$ ;

$\mathcal{H} \leftarrow$  output of (25) ;

**if**  $\mathcal{H} = \tilde{\mathcal{H}}_0$  **then**

            Reject  $\leftarrow 0$ ,  $\hat{\alpha}_b \leftarrow \alpha$

**else**

$t = t + 1$ ;

$\hat{\alpha} \leftarrow \frac{1}{B} \sum_{b=1}^B \hat{\alpha}_b$ ;

---

#### 4.1 Commonly used metrics to analyze model variability

A standard way to analyze variability is by using commonly used metrics like accuracy and churn. The *accuracy* of a model is,

$$A(\theta) = \frac{1}{N_{\text{test}}} \sum_{j=1}^{N_{\text{test}}} \mathbb{1}(\hat{y}(x_j; \theta) = y_j). \quad (26)$$

The *churn* is defined by

$$C(\theta_1, \theta_2) = \frac{1}{N_{\text{test}}} \sum_{j=1}^{N_{\text{test}}} \mathbb{1}(\hat{y}(x_j; \theta_1) \neq \hat{y}(x_j; \theta_2)), \quad (27)$$

which is the fraction of training points where the models disagree. Both accuracy and churn focus on the *predictions* made by models and do not use information about the logit gap function  $m(x; \theta_k)$  beyond its sign. Looking at  $m(x; \theta_k)$  directly gives us other approaches to assess whether models are similar or not: two models may have similar accuracy and low churn but can have very different logit gaps.

We also consider a third metric for the qualitative assessment of these models, the Expected Calibration Error (ECE) [26]. The ECE is a summary statistic of model calibration which measures the difference in accuracy and expected confidence and is obtained by partitioning the predictions into  $R$  equally spaced bins  $B_r$ ,

$$\text{ECE}(\theta) = \sum_{r=1}^R \frac{|B_r|}{N_{\text{test}}} |A(B_r; \theta) - \text{CONF}(B_r; \theta)|, \quad (28)$$

where  $A(B_r; \theta) = \frac{1}{|B_r|} \sum_{j \in B_r} \mathbb{1}(\hat{y}(x_j; \theta) = y_j)$ , and  $\text{CONF}(B_r; \theta) = \frac{1}{|B_r|} \sum_{j \in B_r} \hat{\pi}(y_j = \hat{y}(x_j; \theta) | x_j)$ . A perfectly calibrated model will have  $A(B_r; \theta) = \text{CONF}(B_r; \theta)$ . Although Niculescu-Mizil et al. [27] noted that DNN are well-calibrated on binary classification tasks, it is impossible for a model to achieve perfect calibration in reality, making this another useful metric to assess the quality of models produced through different random seeds in conjunction with accuracy.

## 5 Experiments

Our proposed measure of model closeness/discrepancy offers new insight into questions around neural network training. In this section, we perform a series of illustrative experiments to demonstrate the utility of this measure:

- In Section 5.1, we show that the eCDF of a deep ensemble model reliably approximates the reference as the size of the pool of candidate models in the ensemble increases. Establishing this relationship at the very onset allows us to qualitatively compare candidate models with the deep ensemble substitute of our reference function, while comparing candidate models to the reference function through our robust hypothesis test.
- In Section 5.1.2, we use our proposed measure of model closeness  $\hat{\alpha}$  to show the minimum number of candidate models needed to form a reliable deep ensemble that has less variability in different performance metrics and approximates our reference function well. We show that the discrepancy measured by the  $\alpha$ -trimming levels computed by our proposed test between an ensemble model and the average of the eCDFs of those same models decreases as the number of models in the ensemble pool increases.
- In Section 5.2, and 5.3, we connect the proposed discrepancy measure to other metrics used to measure network variability. We show how  $\hat{\alpha}$  is more informative than validation accuracy alone through two case studies. The first uses a small CNN to perform a binary classification task on the CIFAR-10 dataset. The second uses a ViT variant, pre-trained on ImageNet, to perform the same task on the same dataset. The former case study allowed us to use neural networks with relatively few parameters, so we can test the limits of the expressivity of the proposed test and the latter to show how the same test applies to large-scale pre-trained models as well.

For experiments in Section 5.1, and 5.2, we chose the following experimental setup. We used a small convolutional neural network with two convolutional layers (having 32 and 16 features, respectively, with a  $3 \times 3$  kernel size) followed by one hidden layer of 64 units and a final layer of 2 units that output the raw logits of the network. Details of the network architecture and parameters are included in Section 7.4.1 of Appendix. We train this network on a subset of the CIFAR-10 dataset [19], under the following setting,

- Out of the 10 classes, we take 8 and create a binary classification problem by merging them into two super groups, with class 1 comprising of airplane, automobile, ship, truck, and class -1 comprising of bird, dog, frog and horse.
- Training set size  $N_{\text{train}} = 40000$  and test size  $N_{\text{test}} = 8000$ .
- We fix all hyper-parameters other than the random seeds by training all models for 50 epochs, with a fixed learning rate of 0.001, and fix the batch size to 32.

We chose a small example to allow us to train many models so we can explore model training in different scenarios. All training runs were performed using the Amarel HPC clusters provided by Rutgers [31]. Code to compute the test statistic and  $\hat{\alpha}$  metric of the two-sample version of the robust KS test has been made available online.<sup>1</sup>

### 5.1 The relation between our reference function and a deep ensemble

This section demonstrates how the eCDF of a deep ensemble model  $\hat{G}_e$  defined in Equation (9), closely approximates our reference function  $\hat{G}$  defined in Equation (8). Establishing this relation will allow us to compare candidate models with the deep ensemble substitute of the reference function using different performance metrics like validation accuracy, churn w.r.t. a deep ensemble, and the expected calibration error (ECE) while comparing the eCDF of candidate models to the reference function through the robust KS test. A lower ECE indicates a better-calibrated model, while lower churn w.r.t. an ensemble indicates less disagreement between candidate models and an ensemble. We point the readers to Section 4.1 for a formal definition of these metrics. We train a total of

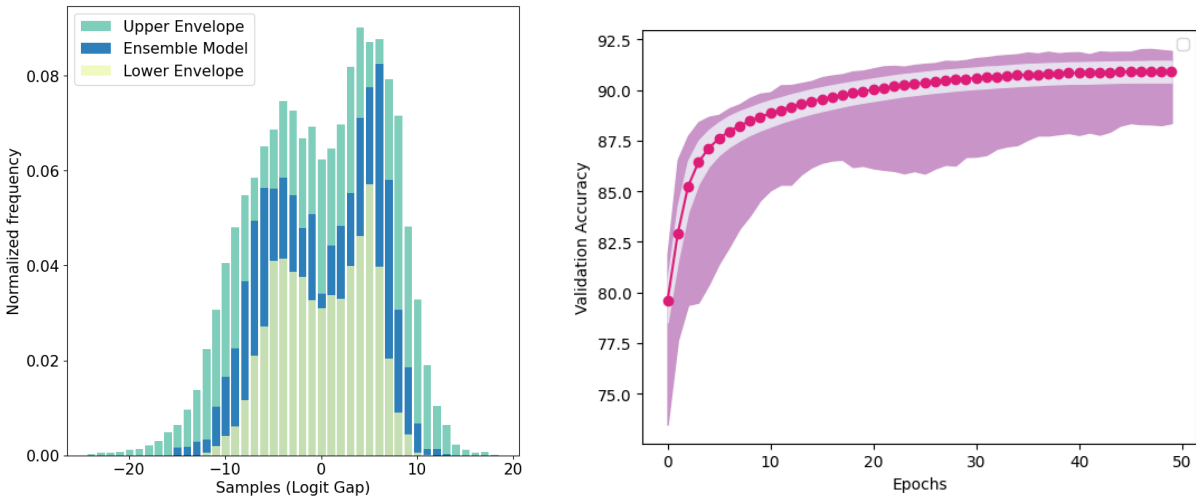


**Figure 3:** (Left) Histogram of logit gaps from the ensemble model with the upper and lower envelopes representing the maximum and minimum probability attained in each bin among individual candidate models. (Right) A plot showing the evolution of validation accuracy of candidate models over different epochs. The solid red dots represent the mean of validation accuracy over 800 seeds at each epoch, the light-colored area represents one standard deviation, and the purple area represents the maximum and minimum values at that epoch.

1600 models by randomly fixing a seed for each model. The seeds control both initialization and batch order during SGD. We use the first  $M = 800$  models to create a reference function  $\hat{G}$  and set the rest  $M' = 800$  models to create the eCDF of a deep ensemble  $\hat{G}_e$ . We choose different ensemble sizes  $P \in [3, 5, 10, 20, 30, 70, 100, 150, 200]$  to observe the variability of ensembles in different metrics and to understand how large of an ensemble we need to approximate the reference function well. For each value of  $P$ , we sample  $P$  models without replacement from the remaining  $M' = 800$  models and compute  $\hat{G}_e$ . We repeat this experiment 500 times to get 500 ensemble models using  $P$  components for each value of  $P$ . Deep ensemble predictors have been widely used in the literature to reduce variability in DNN models [20, 21]. Candidate models will have varying degrees of certainty on individual test points. Taking the average of model “confidences” across independent training runs makes them closer to their expected values, lowering variability. Although ensembling through

<sup>1</sup><https://github.com/kanupolo10/SIGNAL/experiments/Robust-KS-Tests>

averaging over softmax probabilities is common practice in the literature, averaging over logits has also been investigated to address the shortcomings of probability averaging [15, 34].

Figure 3 (Left) shows how the logit gap samples obtained from ensembling  $P = M'$  candidate models compare with candidate models in the pool. The ensemble model produces fewer samples with small logit gaps (samples with higher uncertainty) and large logit gaps (overconfident samples).

Figure 3 (Right) shows the evolution of validation accuracy of candidate models over epochs. The solid red dots in the plot correspond to the mean accuracy over  $M'$  seeds at each epoch, the light-colored region corresponds to one standard deviation, and the purple region corresponds to the minimum and maximum accuracy at that epoch. As observed in the plot, validation accuracy stops increasing from epoch 30 onwards, hence the decision to stop training at epoch 50, which is well past this optimization convergence. The same strategy was adopted by Picard to study deep net variability; see [28, Section 4.1] for a discussion on this.

### 5.1.1 Closeness of a deep ensemble to the reference function

The first question we want to answer is **how quickly does the eCDF of an ensemble model approximate the chosen reference?** In other words, as  $P$  approaches  $M'$  how quickly does  $\|\hat{G} - \hat{G}_e\|_\infty$  decrease? To answer this, we compute the  $L_\infty$ -distance between  $\hat{G}$  and  $\hat{G}_e$  and compare it to the threshold set by the test in Equation (13). To set the threshold  $\delta_a$  in Equation (14), we fix  $\epsilon_a = 0.01$ .

Figure 4 demonstrates this convergence behavior. The eCDF of all ensemble models  $\hat{G}_e$ , produced with  $P = 100, 150,$  and  $200$  candidate models have  $L_\infty$ -distances from  $\hat{G}$  less than the threshold set for our KS test. This empirical evidence indicates that a deep ensemble eCDF more closely resembles the reference function  $\hat{G}$  as  $P$  approaches  $M'$ . Therefore, we expect any candidate model close to our reference function  $\hat{G}$ , formed with  $M$  candidate models, to be also close to a deep ensemble, formed with  $P$  candidate models, in terms of different performance metrics, provided  $P$  approaches  $M' = M$ . When analyzing the variability of candidate models, we use the robust KS test for comparing the closeness of the eCDF of each candidate model to the reference function  $\hat{G}$ , and use the deep ensemble substitute of this reference function for qualitative comparison with candidate models.

Since the benefits of ensembling are observed even for pool sizes as small as  $P = 5$  [20], it might be tempting to focus on a few random seeds to generate a deep ensemble model due to computational constraints. This brings us to the next question: **Does averaging over a small number of candidate models to create an ensemble model result in a reliable representative of the training procedure?** We try to understand this qualitatively. We investigate three metrics of ensemble models as  $P$  approaches  $M'$ : validation accuracy, churn w.r.t. a deep ensemble of pool size  $P = M$ , and ECE. In Figure 5, we use a 3-D scatter plot to visualize the relation among the ensemble models w.r.t. these three metrics. We expect the best ensembles to have high validation accuracy, low churn, and low ECE.

As observed in Figure 5, there is a cluster of ensembles that all have high accuracy, low churn, and low ECE, which is the desired behavior. These “good” ensembles are almost all created from a large number of models. These are also the same models whose eCDFs have achieved a smaller  $L_\infty$ -distance from the reference function  $\hat{G}$  in Figure 4. Some ensembles created from a small number of models may outperform those created from a large number of models in one particular metric, but it is always at the cost of performance w.r.t. another metric. For instance, one of the highest validation accuracy achieved in Figure 5 is an ensemble model belonging to  $P = 5$ . However, this model also has a higher churn w.r.t. an ensemble of size  $P = M$ . This is also reflected by the high  $L_\infty$ -distance of this model from the reference  $\hat{G}$  as shown in Figure 4. We conclude that contrary

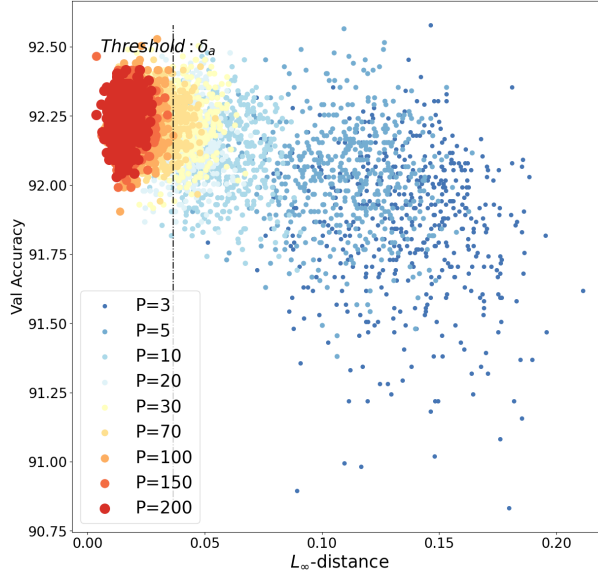


**Figure 4:** A plot showing  $L_\infty$ -distance of the eCDF of ensemble models  $\hat{G}_e$  (formed with  $P$  models) w.r.t. the reference  $\hat{G}$  (formed with  $M$  models) against validation accuracy of ensemble models. For each value of  $P$ , we choose  $P$  candidate models to form one ensemble model and repeat this experiment 500 times through sampling with replacement to create 500 ensemble models. Thus, each dot with a fixed color represents one out of these 500 ensemble models and each color indicates the value of  $P$  or the number of candidate models in the pool. We chose  $\epsilon = 0.01$ , to compute the threshold  $\delta_a$  in Equation (14).

to standard practice, exploring more than 5 seeds is important to create a reliable ensemble that has less variability in different performance metrics. Thus, **ensembling over smaller pool sizes results in a deep ensemble that has significant variability over different metrics used to evaluate model performance, and increasing the size  $P$  of ensemble models reduces this variability.**

### 5.1.2 Selecting the number of models to be ensembled via the robust KS test

Section 5.1.1 showed that it is possible to create a good ensemble with enough models that have less variability over different performance metrics and whose eCDF approximates the reference function well. The more models we ensemble, the better and more consistent the ensembles become. This brings us to our final question: **How many candidate models do we need to create a deep ensemble model that is a reliable representative of the training procedure i.e. has less variability over different performance metrics and approximates the reference function well?** Based on the threshold set by our test on the  $L_\infty$ -distance and as demonstrated in Figure 4, a classical KS test will indicate that we need to explore 100 random seeds to create a reliable ensemble, which can then be used as a base model for qualitative comparisons with candidate models. Since the classical KS test is too sensitive, setting a threshold based on it will require too many models to create the ensemble. We can use the proposed robust KS test to also measure the similarity between the ensemble function  $\hat{G}_e$  and the reference function  $\hat{G}$  but with a little wiggle room. In practice, we also may not want to rely on validation accuracy or churn to decide on the number of models we need. So, the proposed test offers a way to estimate this number using only the logits. To that end, we compute  $\hat{\alpha}$  through a robust KS test to measure the closeness/discrepancy of the eCDFs of ensemble models  $\hat{G}_e$ , of different sizes, with the reference function  $\hat{G}$ . Similar to Figure 4, in Figure 6, as  $P$  approaches  $M'$ ,  $\hat{\alpha}$  approaches 0. However, if we set a threshold on the

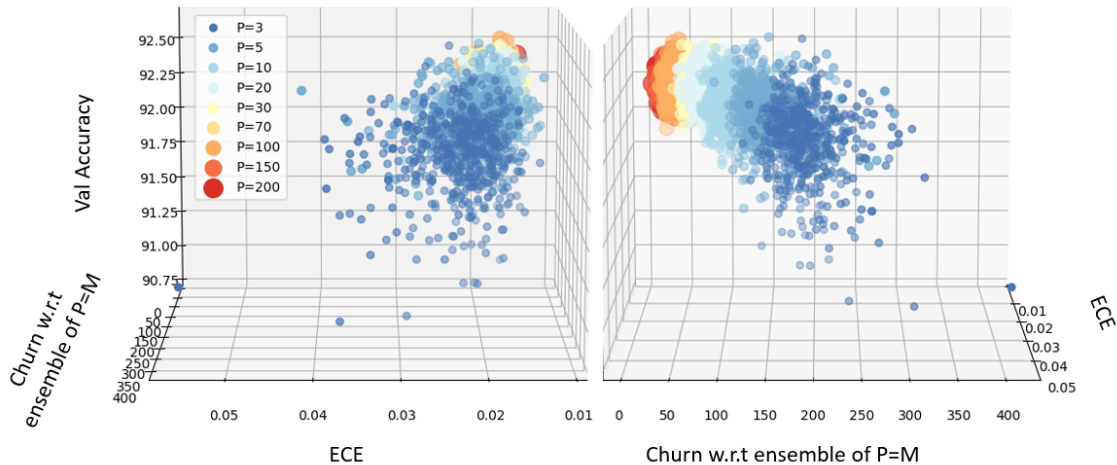


**Figure 5:** 3-D scatter plot to visualize the relationship among ensemble models in terms of validation accuracy, ECE, and churn w.r.t. an ensemble of size  $P = M$ . For each value of  $P$ , we choose  $P$  candidate models to form one ensemble model and repeat this experiment 500 times through sampling with replacement to create 500 ensemble models. Thus, each dot with a fixed color represents one out of these 500 ensemble models and each color indicates the value of  $P$  or the number of candidate models in the pool.

$\alpha$ -trimming level instead of the  $L_\infty$ -distance, we get a better lower bound on the number of models we need to use for a reliable ensemble. If we consider all ensembles that require  $\hat{\alpha} \leq 0.05$ , we see that ensembles created from  $P = 30$  models or more are all included in this set as shown in column 2 of Table 1, while more than 20% of ensembles created from  $P = 3$  models have required a higher level of trimming. From Table 1, we notice that ensembles achieve better values in all metrics as the size of the ensemble  $P$  increases and the variability of these three metrics reduces noticeably for ensembles created from  $P = 30$  models or more. **Thus, our proposed metric indicates that ensembling over at least  $P = 30$  candidate models may be required for an ensemble to be a reliable representative of the training variability.**

<b>P</b>	<b>% of models with <math>\hat{\alpha} \leq 0.05</math></b>	<b>Accuracy mean <math>\pm</math> std</b>	<b>Churn w.r.t. ensemble of size <math>P = M</math> mean <math>\pm</math> std</b>	<b>ECE mean <math>\pm</math> std</b>
3	77.20	91.85 $\pm$ 0.25	190.79 $\pm$ 33.90	0.0226 $\pm$ 0.0048
5	89.20	92.03 $\pm$ 0.18	145.70 $\pm$ 28.61	0.0200 $\pm$ 0.0037
10	96.80	92.11 $\pm$ 0.14	103.57 $\pm$ 22.50	0.0185 $\pm$ 0.0023
20	99.40	92.17 $\pm$ 0.11	76.972 $\pm$ 17.23	0.0175 $\pm$ 0.0016
30	100.00	92.21 $\pm$ 0.10	62.84 $\pm$ 12.45	0.0171 $\pm$ 0.0014
70	100.00	92.22 $\pm$ 0.08	43.45 $\pm$ 9.64	0.0168 $\pm$ 0.0012
100	100.00	92.23 $\pm$ 0.08	38.59 $\pm$ 9.08	0.0169 $\pm$ 0.0012
150	100.00	92.23 $\pm$ 0.07	32.75 $\pm$ 7.42	0.0169 $\pm$ 0.0011
200	100.00	92.24 $\pm$ 0.07	29.3 $\pm$ 6.91	0.0169 $\pm$ 0.0011

**Table 1:** Table showing ensemble statistics for different values of  $P$

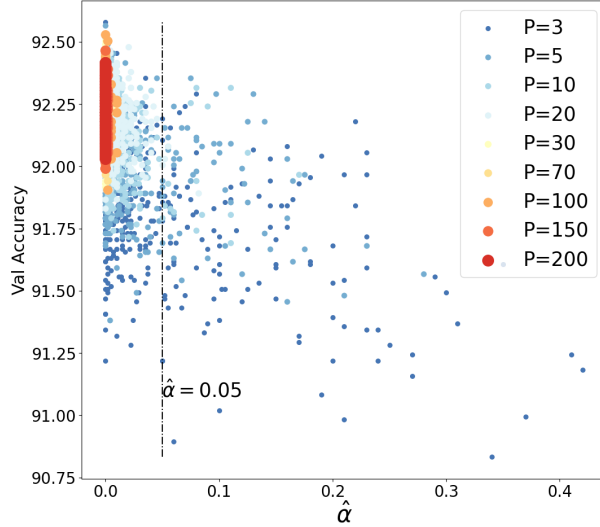


**Figure 6:** A plot showing  $\hat{\alpha}$  of the eCDF of ensemble models  $\hat{G}_e$  (formed with  $P$  models) w.r.t. the reference  $\hat{G}$  (formed with  $M$  models) against validation accuracy of ensemble models. For each value of  $P$ , we choose  $P$  candidate models to form one ensemble model and repeat this experiment 500 times through sampling with replacement to create 500 ensemble models. Thus, each dot with a fixed color represents one out of these 500 ensemble models and each color indicates the value of  $P$  or the number of candidate models in the pool.

## 5.2 Evaluating our proposed metric of model closeness/discrepancy

We next move on to understand how our proposed measure of model closeness/discrepancy relates to metrics commonly used to understand model variability. We try to understand this for candidate models generated under different sources of randomness (like initialization and batch order). In particular, we considered three scenarios:  $S_{\text{init}}$  with only random initialization and fixed batches,  $S_{\text{batch}}$  with only random batch selection in SGD and fixed initialization, and  $S_{\text{all}}$  combining both sources of randomness. We trained 200 models in each of  $S_{\text{init}}$ ,  $S_{\text{batch}}$ , and  $S_{\text{all}}$  with the same hyper-parameter settings as detailed at the beginning of Section 5. For each source of randomness, we use  $M = 100$  models to create the reference function  $\hat{G}$  as defined in Equation (8) and choose our candidate models with eCDF  $\hat{G}_k$  as defined in Equation (5) from the rest  $M' = 100$  models. For each candidate model, we use its eCDF  $\hat{G}_k$  to compute  $\hat{\alpha}$  through a robust KS test against the reference  $\hat{G}$ .

### 5.2.1 Comparing our proposed discrepancy measure with accuracy

Our first question in this section is: **How does our proposed metric  $\hat{\alpha}$  relate to accuracy?** In Figure 7, we plot the relationship between the validation accuracy of candidate models and  $\hat{\alpha}$  for candidate models in  $S_{\text{init}}$ ,  $S_{\text{batch}}$ , and  $S_{\text{all}}$ . For each plot, we notice significant variability over random seeds in both  $\hat{\alpha}$  and validation accuracy for the same hyper-parameter setting. This is evidence that a fixed hyper-parameter setting that works well for one random seed can perform poorly for another and thus produce models with very different logit gap functions. We notice more variability in both validation accuracy and  $\hat{\alpha}$  among models in  $S_{\text{batch}}$ , than models in  $S_{\text{init}}$ . Details of accuracy statistics for each source of randomness are listed in Table 2. The mean accuracy of models in  $S_{\text{init}}$  is slightly higher than models in  $S_{\text{all}}$ , and  $S_{\text{batch}}$ , while all three categories have achieved similar maximum accuracy. The higher variability among models in  $S_{\text{batch}}$  comes from producing models with much poorer validation accuracy than  $S_{\text{init}}$ , a trend also observed in  $S_{\text{all}}$



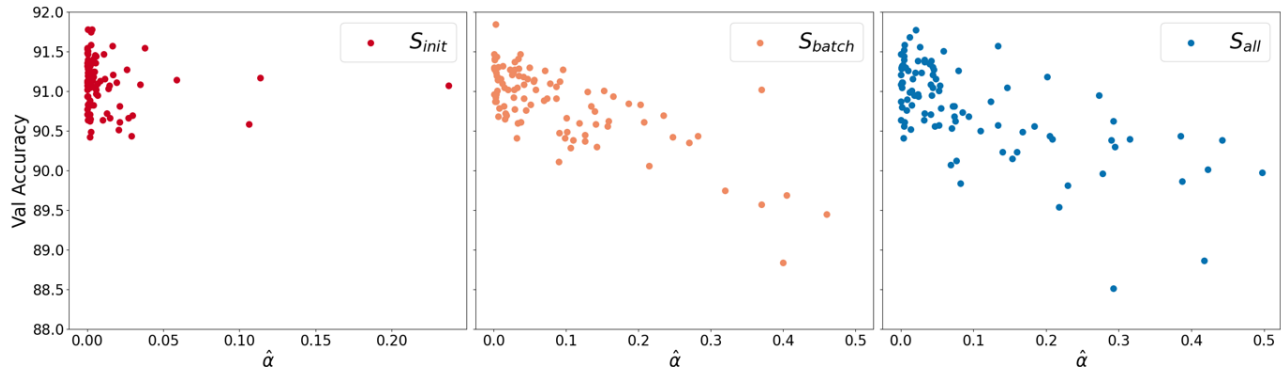


**Figure 7:** 2-D Scatter plot to visualize the relationship of candidate models with their average cdf,  $\hat{G}$ , in terms of validation accuracy and  $\hat{\alpha}$  for models in  $S_{init}$ ,  $S_{batch}$  and  $S_{all}$ .

Random Sources	Accuracy mean + - std	Accuracy range	Ensemble Accuracy	Accuracy range of models with $\hat{\alpha} \leq 0.05$
$S_{init}$	91.101 + 0.302 -	[90.422, 91.781]	91.731	[90.422, 91.781]
$S_{batch}$	90.819 + 0.554 -	[87.852, 91.843]	91.731	[90.409, 91.843]
$S_{all}$	90.810 + 0.560 -	[88.513, 91.769]	92.361	[90.409, 91.769]

**Table 2:** Validation Accuracy statistics of candidate models generated from different random sources:  $S_{init}$ ,  $S_{batch}$ , and  $S_{all}$  along with the ensemble accuracy for each random source.

as reported in the minimum accuracy of the accuracy range for each category. This indicates that random batch shuffling has a higher effect on the overall variability among models in  $S_{all}$ , than random initialization. We also notice that although there is more variability among models in  $S_{batch}$ , than  $S_{init}$ , the ensemble model has performed the same for both categories. However, the combined variability of  $S_{init}$ , and  $S_{batch}$ , reflected among models in  $S_{all}$  has led to a better ensemble performance in  $S_{all}$ .

We also look at models admitted by small values of  $\hat{\alpha}$  in each category (e.g.  $\hat{\alpha} \leq 0.05$ ), and observe the corresponding range of validation accuracy, reported in the fourth column of Table 2. For  $S_{init}$ , the range of accuracy achieved by models admitted by  $\hat{\alpha} \leq 0.05$  covers the full range of accuracy of all models in  $S_{init}$ . This range is also close to the range of models admitted by  $\hat{\alpha} \leq 0.05$  in  $S_{all}$ , and  $S_{batch}$ . The maximum validation accuracy for each source is also admitted by small values of  $\hat{\alpha}$ . This is because candidate models aggregate to form ensembles that result in a boost over average performance in the group. Since models with lower  $\hat{\alpha}$  are close to the reference function in terms of their eCDF, and hence also to the ensemble, they will also have accuracy similar to the ensemble. For each source of randomness, if we consider the range of validation accuracy for models admitted by small values of  $\hat{\alpha}$  to be representative of the training variability (as a result of being close to the reference function), then any model that has performed worse than this range will end up with a high value of  $\hat{\alpha}$ . This can be observed for  $S_{batch}$ , and  $S_{all}$  since these two categories have resulted in more models with performance worse than the discussed range. However, the opposite is not true, i.e. models with accuracy within the discussed range will not always have a small  $\hat{\alpha}$ , and hence will not be good representatives. This shows that validation accuracy alone is not the right metric to assess model quality. A model can end up within the discussed range of validation accuracy but not be a good representative of the training variability over random seeds.



We conclude that lower  $\hat{\alpha}$  does not admit poor validation accuracy, but similar validation accuracy does not imply similar  $\hat{\alpha}$ .

### 5.2.2 Comparing our proposed discrepancy measure with pairwise churn

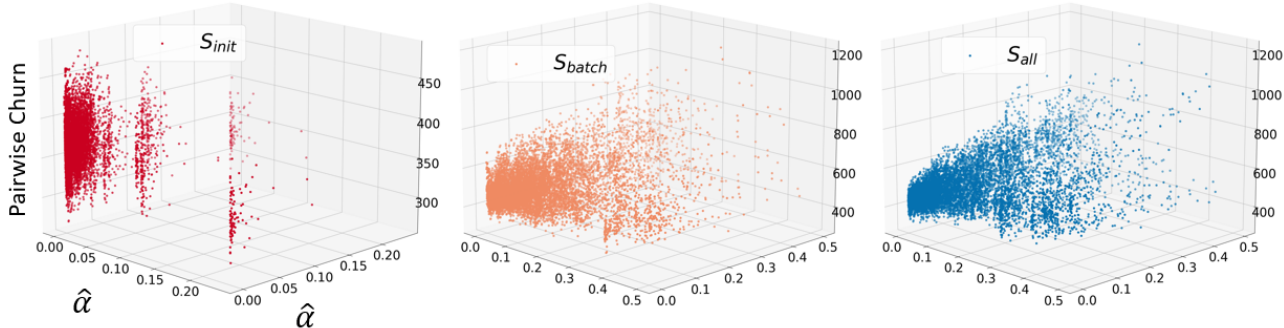


Figure 8: 3-D scatter plot to visualize the relationship of candidate models with their average cdf,  $\hat{G}$ , in terms of pairwise churn and  $\hat{\alpha}$ , for models in  $S_{init}$ ,  $S_{batch}$  and  $S_{all}$

Random Sources	Range of pairwise churn	Range of pairwise churn of pairs of models with $(\hat{\alpha}_i \leq 0.05, \hat{\alpha}_j \leq 0.05), i \neq j$
$S_{init}$	[270, 481 ]	[270, 481 ]
$S_{batch}$	[218, 1174 ]	[ 283, 467]
$S_{all}$	[327, 1184 ]	[283, 462]

Table 3: Pairwise churn statistics of models generated from different random sources:  $S_{init}$ ,  $S_{batch}$ , and  $S_{all}$

**How does our proposed metric  $\hat{\alpha}$  relate to pairwise churn?** In Figure 8, we plot the relationship between the pairwise disagreement between candidate models or churn, and  $\hat{\alpha}$ , for candidate models in  $S_{init}$ ,  $S_{batch}$ , and  $S_{all}$ . We distinguish this from churn w.r.t. a deep ensemble by labeling it as pairwise churn. Similar to the trend observed for validation accuracy, there is more variability in pairwise churn among pairs of models in  $S_{init}$ , than  $S_{batch}$ , as observed in the pairwise churn range for each random source reported in column 2 of Table 3. Again, most of the variability in pairwise churn in  $S_{all}$  is due to  $S_{batch}$ . For all plots in Figure 8, we observe that pairs of models with lower values of  $\hat{\alpha}$  have achieved a smaller range of pairwise churn among its group. This is less obvious for models in  $S_{init}$ , because this group’s total range of pairwise churn is low. We see this in column 3 of Table 3, where we focus on pairs of models in each category that have achieved pairwise  $\hat{\alpha}$  less than 0.05 and report the range of pairwise churn for those models. Since the range of pairwise churn of pairs of models in  $S_{init}$  is low, small values of pairwise  $\hat{\alpha}$  have admitted this full range. We also see that the pairs of models admitted by small values of  $\hat{\alpha}$  in  $S_{batch}$ , and  $S_{all}$  have a pairwise churn range close to the pairwise churn range admitted by small values of  $\hat{\alpha}$  in  $S_{init}$ . Any pairs of models with pairwise churn higher than this range will have at least one model in the pair with a high  $\hat{\alpha}$ . A possible explanation for a pair of models with low pairwise  $\hat{\alpha}$  also having a low pairwise churn is that, models with low  $\hat{\alpha}$  are expected to consist of “good” models that are similar to a good quality ensemble. Since these models achieve validation accuracy within a higher range among their group, the number of points they will make mistakes on will be low.

This will also result in a low pairwise churn because these models will only have a limited number of test points to disagree on. As observed for validation accuracy, the opposite is again not true for pairwise churn, i.e., models with low pairwise churn will not necessarily have small values of pairwise  $\hat{\alpha}$ . Higher values of  $\hat{\alpha}$  will include models with both high and low validation accuracy, resulting in either high or low pairwise churn. We conclude that **lower pairwise  $\hat{\alpha}$  does not admit high pairwise churn but low pairwise churn does not imply lower pairwise  $\hat{\alpha}$ .**

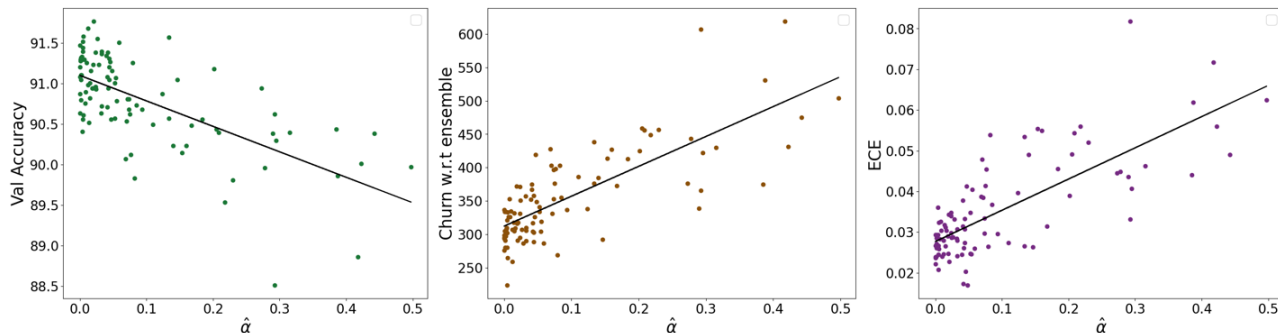
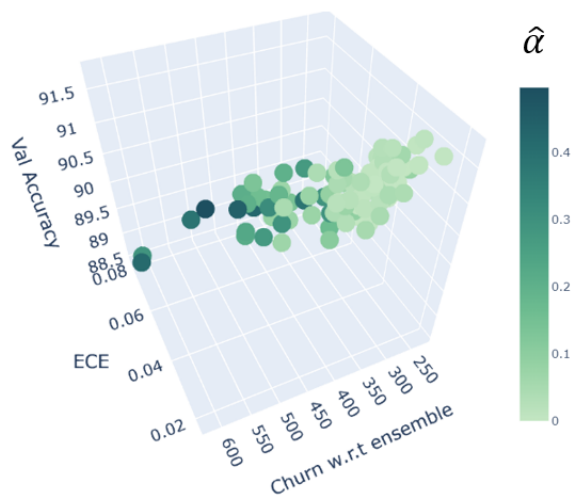


**Figure 9:** 2-D scatter plot to visualize the relationship of  $\hat{\alpha}$  of candidate models in  $S_{\text{all}}$  with their average cdf,  $\hat{G}$ , in terms of (Left) Validation accuracy, (Middle) Churn w.r.t. their ensemble and (Right) ECE.

### 5.2.3 Our proposed discrepancy measure is more informative than accuracy



ECE	Churn w.r.t. ensemble	Val Accuracy	Average Churn	$\hat{\alpha}$
0.021	280	91.519	458.61	0.005
0.023	318	91.769	476.95	0.021
0.026	376	91.569	<b>513.83</b>	<b>0.134</b>
0.029	307	91.556	476.35	0.027
0.030	371	91.382	482.45	0.024
0.026	265	91.581	459.37	0.005
0.030	309	91.157	475.91	0.016
0.028	297	91.108	472.15	0.002
<b>0.038</b>	<b>425</b>	91.182	<b>552</b>	<b>0.201</b>

**Figure 10:** 3-D scatter plot to visualize how  $\hat{\alpha}$  compares to other metrics for 100 candidate CNN models performing a binary classification task on CIFAR-10. **Figure 11:** Table showing  $\hat{\alpha}$  values for CNN models with similar validation accuracy and their corresponding values achieved in other metrics.

We now provide evidence that  $\hat{\alpha}$  is more informative than validation accuracy for model comparison. Figure 9 and Figure 10 show the relationship of  $\hat{\alpha}$  of candidate models in  $S_{\text{all}}$  with three metrics: validation accuracy, churn w.r.t the ensemble of candidate models, and their ECE, in 2-D and 3-D respectively. If the eCDF of a candidate model is close to the eCDF of the reference function, i.e. for smaller values of  $\hat{\alpha}$  the variability in each of the three metrics is confined to a range that includes the best value in each metric, with the worst value not differing too much from the best value. For each metric, we can think of the range of values corresponding to a low  $\hat{\alpha}$  as the

minimum variability observed in models that are close to their expected distribution. Any model that has achieved a value worse than this range will also have a high  $\hat{\alpha}$ . Models with low  $\hat{\alpha}$  are within a higher accuracy range among their group and have ECE and churn w.r.t. ensemble within a low range. However, the converse is not true, i.e. high accuracy or low churn w.r.t. ensemble or low ECE alone does not imply low  $\hat{\alpha}$ . These models can achieve a value that is within a good range of values in one metric but can perform poorly in another metric, and this is reflected in the corresponding  $\hat{\alpha}$  value. To see this, we focus on models that have achieved a similar high validation accuracy and look at other metrics like ECE, average churn for each model w.r.t. all other models, and churn w.r.t. their ensemble in Table 11.  $\hat{\alpha}$  is low if all three metrics fall within the previously discussed good range of values. An increase in  $\hat{\alpha}$  (denoted in bold) in Table 11 indicates a reduction in quality in one or more of these metrics. We can see that most models with similar validation accuracy in Table 11 have needed only a small trimming level ( $\hat{\alpha} \leq 0.05$ ) to not reject the null. But in row 3 and row 9, we see that despite having similar validation accuracy,  $\hat{\alpha}$  values are large due to a reduction in quality in other metrics (denoted in bold).

### 5.3 Application in Transfer Learning

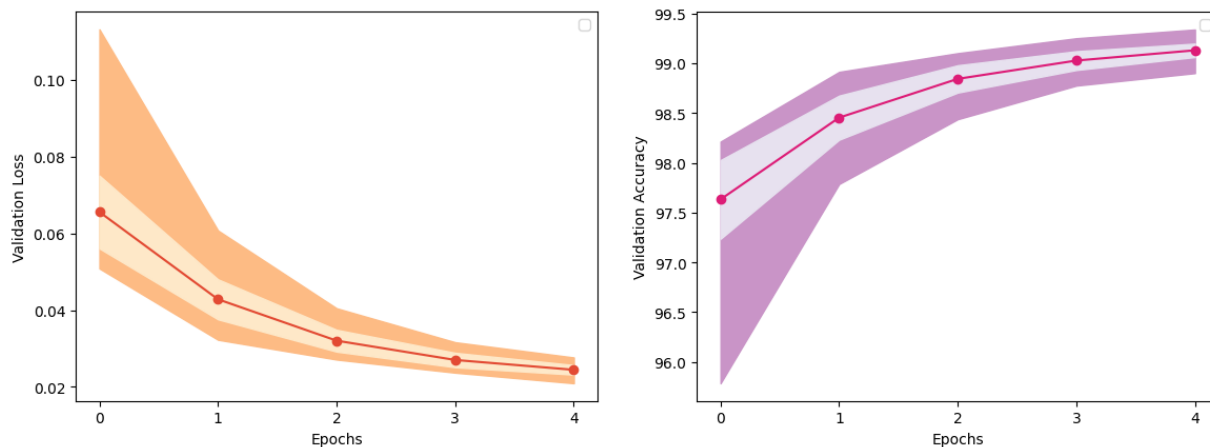


**Figure 12:** (Left) Validation loss vs epochs of ViT models, pre-trained on ImageNet, and performing binary classification task on CIFAR10. The solid red dots represent the mean of validation loss over 45 seeds at each epoch, the light-colored area represents one standard deviation, and the orange area represents the maximum and minimum values at that epoch. (Right) Validation accuracy vs epochs of ViT models pre-trained on ImageNet and performing binary classification task on CIFAR10. The solid red dots represent the mean of validation accuracy over 45 seeds at each epoch, the light-colored area represents one standard deviation, and the purple area represents the maximum and minimum values at that epoch.

We conclude our experiments by demonstrating the usefulness of our framework in transfer learning. We use a Vision Transformer (ViT) variant [22], pre-trained on ImageNet, to perform a downstream binary classification task on CIFAR-10 (as described in Section 5). The pre-trained model is available as part of the Hugging Face Community [23]. We only train the final task-specific classification layer for 5 epochs (till close to convergence as visualized in Figure 12) and rely on already fine-tuned hyper-parameters and the pre-trained weights of the upstream task to “fine-tune” the downstream binary classification task over random seeds only. Thus, keeping the fine-tuning regime and pre-trained weights fixed, we only vary the random seed that controls different sources of randomness in the training procedure (initialization and batch order during SGD), generate 90 models, and observe the variability over random seeds for this fixed setup. As observed by Picard

et al. [28], there is less variability in validation accuracy over random seeds when using pre-trained models.

We create our reference function  $\hat{G}$  as defined in Equation (8), using the first 45 models and treat the rest 45 models as our candidate models  $\hat{G}_k$  as defined in Equation (5), for comparison with the reference. We conduct the same experiment as in Section 5.2.3, where we run our robust hypothesis test between the reference function  $\hat{G}$  and candidate models  $\hat{G}_k$  to compute our proposed discrepancy measure  $\hat{\alpha}$ . Following similar reasoning to Section 5.2.3, in Figure 13, we observe how our proposed metric is more informative than validation accuracy.  $\hat{\alpha}$  is indicative of the quality of models in terms of other metrics like ECE, churn w.r.t. an ensemble and average churn of candidate models w.r.t. all other models in the pool alongside accuracy. A higher  $\hat{\alpha}$  is usually accompanied by a reduction in quality in one or more of these three metrics, denoted in bold in Table 14. Although pre-trained large-scale models provide us with very high validation accuracy and less variability in different metrics used to assess model performance when fine-tuned over the final classification layer, our experiment demonstrates how low values of  $\hat{\alpha}$  are still useful in identifying the best representatives of the training procedure.

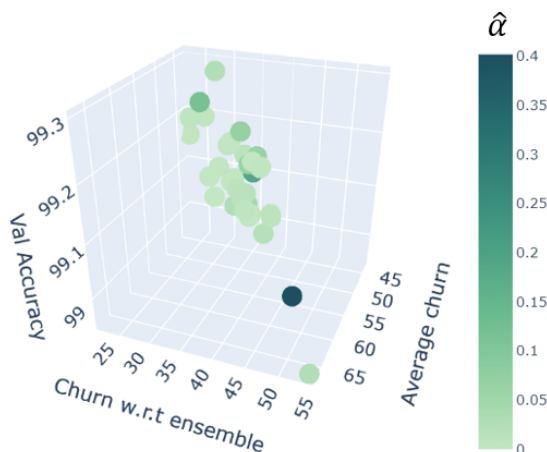


Figure 13: 3-D scatter plot to visualize how  $\hat{\alpha}$  compares to other metrics for 45 candidate ViT models pre-trained on ImageNet for a binary classification task on CIFAR-10. Each dot represents one candidate model.

Average churn	Churn w.r.t. ensemble	Val accuracy	ECE	$\hat{\alpha}$
48.33	30	99.3	0.002	0.026
<b>49.44</b>	28	99.25	<b>0.003</b>	<b>0.118</b>
45.88	24	99.2	0.001	0.007
44.82	26	99.2	0.002	0.004
47.97	<b>34</b>	99.2	0.001	<b>0.069</b>

Figure 14: Table showing  $\hat{\alpha}$  values for candidate models with similar validation accuracy and their corresponding values achieved in other metrics.

Through these experiments, we highlight the importance of treating seeds controlling random elements in a DNN architecture as a separate hyper-parameter that needs “tuning” and propose a framework to reliably select seeds that do not rely solely on commonly used performance metrics like validation accuracy. For practitioners interested in a good seed selection to account for the variability caused by random seeds, the recommendation is to explore at least 30 seeds and choose the seed that generates a model with high validation accuracy and low  $\hat{\alpha}$ .

## 6 Conclusion and Future Work

In this work, we propose a framework for random seed selection of a DNN with a fixed architecture and a fixed hyper-parameter setting. Our proposed framework is based on a robust two-sample hypothesis testing problem that uses trimming of the eCDF of samples obtained from the logit gap function. Our test assesses the closeness of candidate models in a pool with their expected eCDF by down-weighting that part of the data that has a greater influence on the dissimilarity. We also

provide some evidence that our new measure, the trimming level  $\hat{\alpha}$ , could be a more informative metric to assess model performance than commonly used test/validation accuracy. This allows us to perform random seed selection in a more principled fashion instead of relying solely on trial-and-error methods or metrics like validation accuracy. Since the usefulness of our methodology relies on ensembles achieving significant performance gains over their constituents, we investigate the behavior of the ensemble as the number of models in the ensemble pool increases. Our proposed metric  $\hat{\alpha}$  can also be used as a stopping criterion for the number of different seeds that need to be explored for an ensemble model to reliably approximate the expected eCDF of the logit gap distribution of candidate models, and to have less variability in different performance metrics. Although ensembling by model averaging in the output space is quite straightforward and usually results in performance gains, this comes at the cost of reduced interpretability, since such ensembles do not learn any parameters or features. By selecting models that are close to their ensembles in the output space of a DNN, instead of the ensemble itself, our framework leaves room for model interpretability while at the same time maintaining high accuracy compared to their counterparts. Our methodology can find usefulness in critical application areas like credit risk assessment where a single model is often preferred over the improved accuracy of an ensemble due to interpretability concerns [10].

In scenarios where ensembling by model averaging might not lead to significant performance gains over candidate models in the pool, future extensions of this work include investigating when candidate models form effective ensembles. We are also interested in extensions to multi-class classification and exploring robust two-sample hypothesis testing based on other distance metrics like the Wasserstein metric [3]. In this work, we focused on samples from the logit gap function as our probe to understand deep net variability. We can look at other functions of the trained models, such as the Jacobian or the Neural Tangent Kernel of functions learned by these models. The eigen-distribution of these matrices for instance can inform us how well individual candidate models can generalize to test data.

## References

- [1] P. C. Alvarez-Esteban, E. del Barrio, J. A. Cuesta-Albertos, and C. Matrán. “Trimmed comparison of distributions”. In: *Journal of the American Statistical Association* 103.482 (2008), pp. 697–704. URL: <https://www.jstor.org/stable/27640092>.
- [2] P. C. Álvarez-Esteban, E. del Barrio, J. A. Cuesta-Albertos, and C. Matrán. “Uniqueness and approximate computation of optimal incomplete transportation plans”. In: *Annales de l’IHP Probabilités et statistiques*. Vol. 47. 2. 2011, pp. 358–375.
- [3] P. C. Álvarez-Esteban, E. del Barrio, J. A. Cuesta-Albertos, and C. Matrán. “Similarity of samples and trimming”. In: *Bernoulli* 18.2 (May 2012). ISSN: 1350-7265. DOI: [10.3150/11-bej351](https://doi.org/10.3150/11-bej351). URL: <http://dx.doi.org/10.3150/11-BEJ351>.
- [4] E. del Barrio, H. Inouzhe, and C. Matrán. “On approximate validation of models: a Kolmogorov–Smirnov-based approach”. In: *TEST* 29.4 (2020), pp. 938–965.
- [5] E. d. Barrio, H. Inouzhe, and C. Matrán. “Box-Constrained Monotone Approximations to Lipschitz Regularizations, with Applications to Robust Testing”. In: 187 (2020), pp. 65–87.
- [6] X. Bouthillier, P. Delaunay, M. Bronzi, A. Trofimov, B. Nichyporuk, J. Szeto, N. Mohammadi Sepahvand, E. Raff, K. Madan, V. Voleti, S. Ebrahimi Kahou, V. Michalski, T. Arbel, C. Pal, G. Varoquaux, and P. Vincent. “Accounting for variance in machine learning benchmarks”. In: *Proceedings of Machine Learning and Systems* 3 (2021).

- [7] X. Bouthillier, C. Laurent, and P. Vincent. “Unreproducible Research is Reproducible”. In: *Proceedings of the 36th International Conference on Machine Learning*. Ed. by K. Chaudhuri and R. Salakhutdinov. Vol. 97. Proceedings of Machine Learning Research. PMLR, 2019, pp. 725–734. URL: <https://proceedings.mlr.press/v97/bouthillier19a.html>.
- [8] J. Dodge, G. Ilharco, R. Schwartz, A. Farhadi, H. Hajishirzi, and N. Smith. *Fine-Tuning Pretrained Language Models: Weight Initializations, Data Orders, and Early Stopping*. 2020. arXiv: [2002.06305](https://arxiv.org/abs/2002.06305) [cs.CL].
- [9] A. Dvoretzky, J. Kiefer, and J. Wolfowitz. “Asymptotic minimax character of the sample distribution function and of the classical multinomial estimator”. In: *The Annals of Mathematical Statistics* (1956), pp. 642–669.
- [10] R. Florez-Lopez and J. M. Ramon-Jeronimo. “Enhancing accuracy and interpretability of ensemble strategies in credit risk assessment. A correlated-adjusted decision forest proposal”. In: *Expert Systems with Applications* 42.13 (2015), pp. 5737–5753.
- [11] S. Fort, H. Hu, and B. Lakshminarayanan. *Deep Ensembles: A Loss Landscape Perspective*. Tech. rep. arXiv:1912.02757 [stat.ML]. ArXiv, 2020. DOI: [10.48550/arXiv.1912.02757](https://doi.org/10.48550/arXiv.1912.02757).
- [12] J. D. Gibbons and S. Chakraborti. *Nonparametric Statistical Inference (Sixth Edition)*. Boca Raton, FL, USA: CRC Press, 2021.
- [13] O. E. Gundersen, K. Coakley, C. Kirkpatrick, and Y. Gil. *Sources of Irreproducibility in Machine Learning: A Review*. Tech. rep. arXiv:2204.07610v2 [cs.LG]. ArXiv, Apr. 2023. DOI: [10.48550/arXiv.2204.07610](https://doi.org/10.48550/arXiv.2204.07610).
- [14] P. Henderson, R. Islam, P. Bachman, J. Pineau, D. Precup, and D. Meger. *Deep Reinforcement Learning that Matters*. 2019. arXiv: [1709.06560](https://arxiv.org/abs/1709.06560) [cs.LG].
- [15] G. Hinton, O. Vinyals, and J. Dean. “Distilling the knowledge in a neural network”. In: *arXiv preprint arXiv:1503.02531* (2015).
- [16] P. J. Huber. “Robust estimation of a location parameter”. In: *Breakthroughs in statistics: Methodology and distribution*. Springer, 1992, pp. 492–518.
- [17] P. J. Huber and E. M. Ronchetti. *Robust Statistics, Second Edition*. Hoboken, NJ, USA: John Wiley & Sons, 2009. DOI: [10.1002/9780470434697](https://doi.org/10.1002/9780470434697).
- [18] K. Jordan. *Calibrated Chaos: Variance Between Runs of Neural Network Training is Harmless and Inevitable*. Tech. rep. arXiv:2304.01910 [cs.LG]. ArXiv, 2023. DOI: [10.48550/arXiv.2304.01910](https://doi.org/10.48550/arXiv.2304.01910).
- [19] A. Krizhevsky. *Learning Multiple Layers of Features from Tiny Images*. Tech. rep. Toronto, ON, Canada: University of Toronto, 2009. URL: <https://www.cs.toronto.edu/~kriz/learning-features-2009-TR.pdf>.
- [20] B. Lakshminarayanan, A. Pritzel, and C. Blundell. “Simple and Scalable Predictive Uncertainty Estimation Using Deep Ensembles”. In: *Proceedings of the 31st International Conference on Neural Information Processing Systems*. NIPS’17. Long Beach, California, USA: Curran Associates Inc., 2017, pp. 6405–6416. ISBN: 9781510860964.
- [21] S. Lee, S. Purushwalkam, M. Cogswell, D. Crandall, and D. Batra. *Why M Heads are Better than One: Training a Diverse Ensemble of Deep Networks*. Tech. rep. arXiv:1511.06314 [cs.CV]. ArXiv, 2015.
- [22] Z. Liu, Y. Lin, Y. Cao, H. Hu, Y. Wei, Z. Zhang, S. Lin, and B. Guo. *Swin Transformer: Hierarchical Vision Transformer using Shifted Windows*. 2021. arXiv: [2103.14030](https://arxiv.org/abs/2103.14030) [cs.CV].



- [23] Z. Liu, Y. Lin, Y. Cao, H. Hu, Y. Wei, Z. Zhang, S. Lin, and B. Guo. “Swin Transformer: Hierarchical Vision Transformer using Shifted Windows”. In: *CoRR* abs/2103.14030 (2021). arXiv: [2103.14030](https://arxiv.org/abs/2103.14030). URL: <https://arxiv.org/abs/2103.14030>.
- [24] G. Melis, C. Dyer, and P. Blunsom. *On the State of the Art of Evaluation in Neural Language Models*. 2017. arXiv: [1707.05589](https://arxiv.org/abs/1707.05589) [cs.CL].
- [25] M. Milani Fard, Q. Cormier, K. Canini, and M. Gupta. “Launch and Iterate: Reducing Prediction Churn”. In: *Advances in Neural Information Processing Systems*. Ed. by D. Lee, M. Sugiyama, U. Luxburg, I. Guyon, and R. Garnett. Vol. 29. Curran Associates, Inc., 2016. URL: <https://proceedings.neurips.cc/paper/2016/file/dc5c768b5dc76a084531934b34601977-Paper.pdf>.
- [26] M. P. Naeini, G. Cooper, and M. Hauskrecht. “Obtaining well calibrated probabilities using bayesian binning”. In: *Proceedings of the AAAI conference on artificial intelligence*. Vol. 29. 1. 2015.
- [27] A. Niculescu-Mizil and R. Caruana. “Predicting good probabilities with supervised learning”. In: *Proceedings of the 22nd international conference on Machine learning*. 2005, pp. 625–632.
- [28] D. Picard. “Torch. manual\_seed (3407) is all you need: On the influence of random seeds in deep learning architectures for computer vision”. In: *arXiv preprint arXiv:2109.08203* (2021).
- [29] R. Rahaman and A. H. Thiery. *Uncertainty Quantification and Deep Ensembles*. 2021. arXiv: [2007.08792](https://arxiv.org/abs/2007.08792) [stat.ML].
- [30] N. Reimers and I. Gurevych. *Reporting Score Distributions Makes a Difference: Performance Study of LSTM-networks for Sequence Tagging*. 2017. arXiv: [1707.09861](https://arxiv.org/abs/1707.09861) [cs.CL].
- [31] *Rutgers Office of Advance Research Computing*. <https://oarc.rutgers.edu/resources/amarel/>.
- [32] C. Summers and M. J. Dinneen. *Nondeterminism and Instability in Neural Network Optimization*. Tech. rep. arXiv:2103.04514 [cs.LG]. ArXiv, 2021. DOI: [10.48550/arXiv.2103.04514](https://doi.org/10.48550/arXiv.2103.04514).
- [33] F. Wei and R. M. Dudley. “Two-sample Dvoretzky–Kiefer–Wolfowitz inequalities”. In: *Statistics & Probability Letters* 82.3 (2012), pp. 636–644. ISSN: 0167-7152. DOI: <https://doi.org/10.1016/j.spl.2011.11.012>. URL: <https://www.sciencedirect.com/science/article/pii/S0167715211003658>.
- [34] D. Wood, T. Mu, A. M. Webb, H. W. Reeve, M. Lujan, and G. Brown. “A unified theory of diversity in ensemble learning”. In: *Journal of Machine Learning Research* 24.359 (2023), pp. 1–49.

## 7 Appendix

### 7.1 Analysis

**Theorem 1.** Let  $\hat{G}$  and  $\hat{F}_{\pi|\mathcal{D}_{\text{param}}}$  be given by Equation (8) and (7). Then for any  $\delta_b > 0$ ,

$$\mathbb{P}_{\pi|\mathcal{D}_{\text{param}}}\left(\left\|\hat{F}_{\pi|\mathcal{D}_{\text{param}}} - \hat{G}\right\|_{\infty} > \delta_b\right) \leq \epsilon_b,$$

where  $\epsilon_b = 2M \exp(-2N_{\text{test}}\delta_b^2)$ .

Proof of Theorem 1:

$$\left\| \hat{F}_{\pi|\mathcal{D}_{\text{param}}} - \hat{G} \right\|_{\infty} = \left\| \frac{1}{M} \sum_{k=1}^M \left( \mathbb{E}_{\pi|\theta_k} [\mathbb{1}(m(\mathbf{x}, \theta_k) \leq t)] - \frac{1}{N_{\text{test}}} \sum_{j=1}^{N_{\text{test}}} \mathbb{1}(m(x_j; \theta_k) \leq t) \right) \right\|_{\infty} \quad (29)$$

$$\leq \frac{1}{M} \sum_{k=1}^M \left\| \mathbb{E}_{\pi|\theta_k} [\mathbb{1}(m(\mathbf{x}, \theta_k) \leq t)] - \frac{1}{N_{\text{test}}} \sum_{j=1}^{N_{\text{test}}} \mathbb{1}(m(x_j; \theta_k) \leq t) \right\|_{\infty}. \quad (30)$$

For ease of notation, replace the two terms in the difference of Equation (30) by,

$$A_k(t) \doteq \mathbb{E}_{\pi|\theta_k} [\mathbb{1}(m(\mathbf{x}, \theta_k) \leq t)], \text{ and} \quad (31)$$

$$B_k(t) \doteq \frac{1}{N_{\text{test}}} \sum_{j=1}^{N_{\text{test}}} \mathbb{1}(m(x_j; \theta_k) \leq t) \quad (32)$$

so that,

$$\left\| \hat{F}_{\pi|\mathcal{D}_{\text{param}}} - \hat{G} \right\|_{\infty} \leq \frac{1}{M} \sum_{k=1}^M \|A_k - B_k\|_{\infty}. \quad (33)$$

For each  $\theta_k$ ,  $B_k$  is the eCDF of samples drawn from a distribution with CDF  $A_k$ . By the Dvoretzky-Kiefer-Wolfowitz (DKW) inequality [9],

$$\mathbb{P}_{\pi|\theta_k} (\|A_k - B_k\|_{\infty} > \delta_b) \leq 2 \exp(-2N_{\text{test}}\delta_b^2). \quad (34)$$

Taking a union bound over  $\mathcal{D}_{\text{param}} = \{\theta_k : k \in [M]\}$  we get,

$$\mathbb{P}_{\pi|\mathcal{D}_{\text{param}}} (\exists k \in [M] \text{ s.t. } \|A_k - B_k\|_{\infty} > \delta_b) \leq 2M \exp(-2N_{\text{test}}\delta_b^2). \quad (35)$$

Therefore, each term on the right-hand side of (33) is smaller than  $\delta_b$  w.h.p. and,

$$\mathbb{P}_{\pi|\mathcal{D}_{\text{param}}} \left( \left\| \hat{F}_{\pi|\mathcal{D}_{\text{param}}} - \hat{G} \right\|_{\infty} \leq \delta_b \right) \geq 1 - 2M \exp(-2N_{\text{test}}\delta_b^2), \quad (36)$$

as desired.

## 7.2 Impartial trimming

In section 4, we introduce a robust version of the KS test, where we allow for some outliers in samples from the null hypothesis using  $\alpha$ -trimming of distributions. For completeness purposes, we present the concepts on  $\alpha$ -trimming of a distribution w.r.t. a reference distribution as introduced by Alvarez-Esteban et al. [1]. Trimming allows us to assume some outliers in samples that did come from the null distribution and helps quantify the fraction of these outliers. To elaborate on the concept of trimming, let  $k$  be the number of trimmed observations, and let  $\alpha$  be the trimming fraction, which implies  $k \leq n\alpha$ . Given  $n$  i.i.d samples  $\{x_i\}_{i=1}^n$  with probability distribution  $P$ , the empirical measure can be defined as  $\frac{1}{n} \sum_{i=1}^n \delta^{\text{Dirac}}(x_i)$ , where  $\delta^{\text{Dirac}}(x)$  is the Dirac measure. To not reject the null, we can remove outliers by assigning a weight of 0 to the bad observations in the sample and adjusting the weight of good observations by  $\frac{1}{n-k}$ . However, we may not want to completely get rid of samples from the feasible set and instead downplay the importance of bad



observations by modifying the empirical measure to be  $\frac{1}{n} \sum_{i=1}^n w_i \delta_{x_i}$ , where  $0 \leq w_i \leq \frac{1}{(1-\alpha)}$ , and  $\frac{1}{n} \sum_{i=1}^n w_i = 1$ . This is called an *impartial trimming* of the probability measure  $P$ . Using impartial trimming interchangeably with trimming we look at the definition of  $\alpha$ -trimming, denoted by  $R_\alpha(P)$ , of the distribution  $P$  [1, Definition 1],

$$\mathcal{R}_\alpha(P) = \{P^* \in \mathcal{P} : P^* \ll P, \frac{dP}{dP^*} \leq \frac{1}{(1-\alpha)} P \text{ a.s.}\}. \quad (37)$$

where  $P, P^*$  are probability measures on  $\mathbb{R}$ ,  $0 \leq \alpha \leq 1$ , and we say  $P^*$  is an  $\alpha$ -trimming of  $P$  if  $P^*$  is absolutely continuous w.r.t.  $P$  and satisfies the above definition. The set of  $R_\alpha(P)$ , the  $\alpha$ -trimmings of  $P$ , can be characterized in terms of the trimming function  $h$ . The function  $h$  determines which zones in the distribution  $P$  are downplayed or removed.

Let  $C_\alpha$  be the class of absolutely continuous functions  $h : [0, 1] \rightarrow [0, 1]$ , such that  $h(0) = 0$ , and  $h(1) = 1$ , with derivative  $h'$ , such that  $0 \leq h' \leq \frac{1}{1-\alpha}$ . For any real probability measure  $P$ , the following holds [1, Proposition 1 a.],

$$\mathcal{R}_\alpha(P) = \{P^* \in \mathcal{P} : P^*(-\infty, t] = h(P(-\infty, t]), h \in C_\alpha\}. \quad (38)$$

### 7.3 Trimmed Kolmogorov-Smirnov distance

Given two distribution functions,  $F_{\tau \times \pi}$  and  $G_k$ , the KS distance is given by,

$$d(F_{\tau \times \pi}, G_k) = \sup_{x \in \mathbb{R}} |F_{\tau \times \pi}(x) - G_k(x)|. \quad (39)$$

We analogously define the  $\alpha$ -trimmed KS distance functional as,

$$d(F_{\tau \times \pi}, R_\alpha(G_k)) = \min_{\tilde{F} \in \mathcal{R}_\alpha(G_k)} d(F_{\tau \times \pi}, \tilde{F}). \quad (40)$$

The plug-in estimator for  $d(F_{\tau \times \pi}, R_\alpha(G_k))$  is  $d(F_{\tau \times \pi}, R_\alpha(\hat{G}_k))$ , where  $\hat{G}_k$  is the empirical distribution function based on a sample of  $N_{\text{test}}$  independent random variables with common distribution function  $G_k$ , and  $F_{\tau \times \pi}$  is our null distribution. A practical computation for  $d(F_{\tau \times \pi}, R_\alpha(\hat{G}_k))$  uses function  $F_{\tau \times \pi} \circ G_k^{-1}$  to express  $d(F_{\tau \times \pi}, R_\alpha(G_k))$ . If  $F_{\tau \times \pi}$  is continuous and  $x$  (generated samples) has distribution function  $G_k$ ,  $F_{\tau \times \pi} \circ G_k^{-1}$  is the quantile function associated with the random variable  $Y = F_{\tau \times \pi}(x)$ . This gives rise to the following lemma and theorem for computing the trimmed KS distance between a theoretical distribution and an eCDF [4],

**Lemma 1** ([5], Lemma 2.4). *If  $G_k, F_{\tau \times \pi}$  are continuous distribution functions and  $G_k$  is strictly increasing then,*

$$d(F_{\tau \times \pi}, \mathcal{R}_\alpha(G_k)) = \min_{h \in C_\alpha} \|h - F_{\tau \times \pi} \circ G_k^{-1}\|, \quad d(F_{\tau \times \pi}, \mathcal{R}_\alpha(\hat{G}_k)) = \min_{h \in C_\alpha} \|h - F_{\tau \times \pi} \circ \hat{G}_k^{-1}\|. \quad (41)$$

**Theorem 2** ([5], Theorem 2.5). *Suppose  $\Gamma : [0, 1] \rightarrow [0, 1]$  is a continuous non-decreasing function and let*

$$B(t) = \Gamma(t) - \frac{t}{1-\alpha}, \quad (42)$$

$$U(t) = \sup_{t \leq s \leq 1} B(s), \quad (43)$$

$$L(t) = \inf_{0 \leq s \leq t} B(s), \text{ and} \quad (44)$$

$$\tilde{h}_\alpha(t) = \max \left( \left( \min \left( \frac{U(t) + L(t)}{2}, 0 \right) \frac{-\alpha}{(1-\alpha)} \right), 0 \right). \quad (45)$$

Then

$$h_\alpha \triangleq \tilde{h}_\alpha + \frac{(\cdot)}{(1-\alpha)} \quad (46)$$

is an element of  $C_\alpha$  and  $\min_{h \in C_\alpha} \|h - \Gamma\| = \|h_\alpha - \Gamma\| = \|\tilde{h}_\alpha - \Gamma\|$ , with the assumptions on  $\Gamma$  holding for  $\Gamma = F_{\tau \times \pi} \circ G_k^{-1}$ .

In our application we don't have access to  $F_{\tau \times \pi}$ , and as discussed in Section 4, our robust hypothesis test is against the reference function  $\hat{G}$ . Since this function is an average of eCDFs, which is not a continuous function, for practical computation of  $d(\hat{G}, \mathcal{R}_\alpha(\hat{G}_k))$ , we consider the linearly interpolated cdf of  $\hat{G}$ , which we denote as  $\hat{G}^l$ . Thus running the hypothesis test in Equation (24) is equivalent to running the following test,

$$d(\hat{G}^l, \mathcal{R}_\alpha(\hat{G}_k)) \underset{\mathcal{H}_0}{\overset{\tilde{H}_1}{\geq}} \delta_a + \frac{1}{N_{\text{test}}} \quad (47)$$

or equivalently, from Equation (25),

$$\max_z \min_{\tilde{F} \in \mathcal{R}_\alpha(\hat{G}_k)} |\hat{G}^l(z) - \tilde{F}(z)| \underset{\mathcal{H}_0}{\overset{\tilde{H}_1}{\geq}} \delta_a + \frac{1}{N_{\text{test}}}, \quad (48)$$

where we arrive at the threshold on the right-hand side by considering the inequality  $\|\hat{G} - \hat{G}^l\|_\infty \leq \frac{1}{N_{\text{test}}}$  and then applying the triangle inequality.

## 7.4 Additional Experimental Details

### 7.4.1 CNN architecture

Figure 15 shows the CNN architecture and parameters used in Section 5.

### 7.4.2 Observing the evolution of ensemble models over the training procedure

We once again focus on models in  $\mathcal{S}_{\text{all}}$ , observing the evolution of the ensemble of all candidate models in  $M' = 100$  w.r.t. its constituents at fixed training epochs. We track this evolution w.r.t. our previously used metrics, validation accuracy, ECE, and churn w.r.t. the ensemble. Figure 16 presents four snapshots of this evolution for candidate models and their ensemble in  $\mathcal{S}_{\text{all}}$  at different epochs.

**As candidate models evolve to become more accurate but also over-confident in their predictions, their ensemble also evolves to become a better model:** At smaller epochs, poorly trained candidate models result in ensembles of poor quality. This is evident for epoch 2, and epoch 10 in the top row of Figure 16 where the ensemble of candidate models is of poorer or comparable quality w.r.t. to its constituents in terms of validation accuracy and ECE. As candidate models are trained for longer durations, their ensembles are not only better calibrated but also achieve the highest validation accuracy among their constituents. We also note an overall reduction in the churn of candidate models w.r.t. their ensemble as observed along the x-axis, with increasing epochs, of View 1. This reduction can be attributed to the improvement in the validation accuracy of candidate models over time. However, churn between the ensemble model and its constituents that have achieved the highest range of validation accuracy among its group increases from roughly a range of 180-250 in epoch 10, to 250-400 in epoch 50. This can be explained by the significant

CNN Summary

path	module	inputs	outputs	params
	CNN	float32[39873,32,32,3]	<ul style="list-style-type: none"> <li>- float32[39873,2]</li> <li>- float32[39873,64]</li> <li>- float32[39873,64]</li> <li>- float32[39873,16,16,16]</li> <li>- float32[39873,16,16,32]</li> <li>- float32[39873,32,32,32]</li> </ul>	
CONV1	Conv	float32[39873,32,32,3]	float32[39873,32,32,32]	bias: float32[32] kernel: float32[3,3,3,32]  <b>896 (3.6 KB)</b>
CONV2	Conv	float32[39873,16,16,32]	float32[39873,16,16,16]	bias: float32[16] kernel: float32[3,3,32,16]  <b>4,624 (18.5 KB)</b>
DENSE1	Dense	float32[39873,1024]	float32[39873,64]	bias: float32[64] kernel: float32[1024,64]  <b>65,600 (262.4 KB)</b>
DENSE2	Dense	float32[39873,64]	float32[39873,2]	bias: float32[2] kernel: float32[64,2]  <b>130 (520 B)</b>
			<b>Total</b>	<b>71,250 (285.0 KB)</b>

Total Parameters: 71,250 (285.0 KB)

Figure 15: CNN Architecture

improvement in the validation accuracy of the ensemble compared to its constituents at epoch 50. We also notice an increase in the ECE values of candidate models that have achieved a high range of accuracy in their group, as observed along the x-axis across different epochs in View 2. This is observed as we move from epoch 10 to epoch 50, where the ECE values of the aforementioned group of high-accuracy candidate models decreased roughly from 0.01-0.02 in epoch 10 to 0.02-0.03 in epoch 50. This overconfidence in candidate models that have achieved high accuracy in their group results in a significant improvement in the quality of their ensemble. This non-inherent trait of deep ensembles to be a better-calibrated counterpart of its constituents under the commonly encountered scenario of the pool of candidate models being overconfident was reported by Rahaman et al. [29].

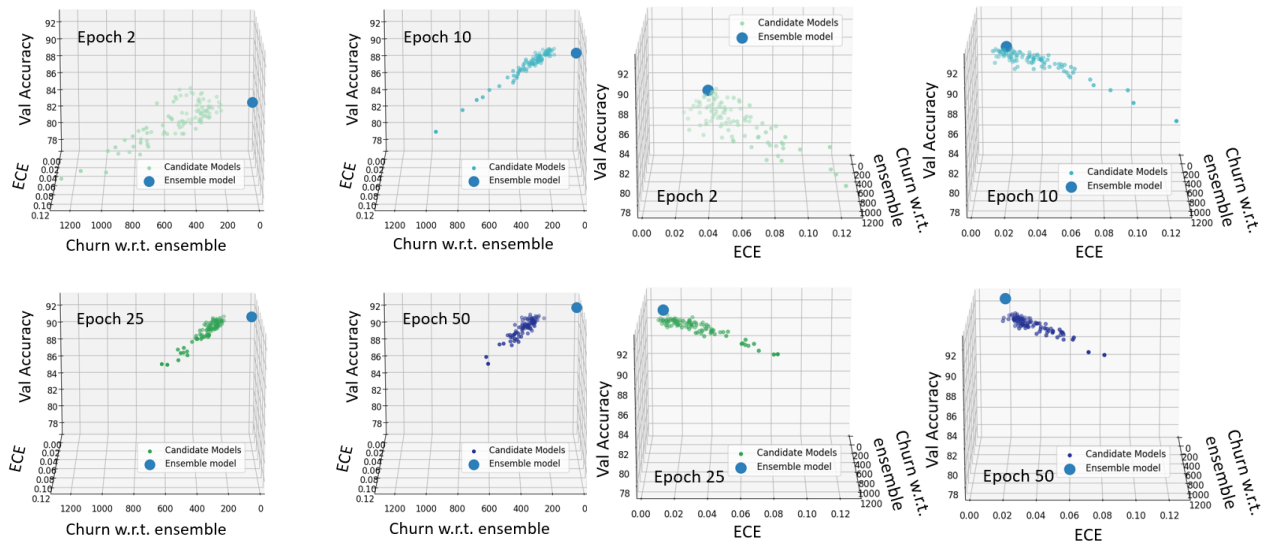


**Figure 16:** 3-D scatter plot with two different views to visualize the relationship of candidate models in  $S_{all}$  at different epochs with their ensemble at that epoch in terms of validation accuracy, ECE, and churn w.r.t. ensemble (Z,Y,X axis) for View 1 (Left) and (Z,X,Y) axis for View 2 (Right).